POLITECNICO DI TORINO
Repository ISTITUZIONALE

Measurement of prompt D+s-meson production and azimuthal anisotropy in Pb-Pb collisions at 5.02 TeV

Original
Measurement of prompt D+s-meson production and azimuthal anisotropy in Pb-Pb collisions at 5.02 TeV / Acharya, S., Adamová, D., Adler, A., Adolfsson, J., Aglieri Rinella, G., Agnello, M., Agrawal, N., Ahammed, Z., Ahmad, S., Ahn, S.U., Ahuja, I., Akbar, Z., Akindinov, A., Al-Turany, M., Alam, S.N., Aleksandrov, D., Alessandro, B., Alfanda, H.M., Alfaro Molina, R., Ali, B., et al.. - In: PHYSICS LETTERS. SECTION B. - ISSN 0370-2693. - ELETTRONICO. - 827:(2022), pp. 1-17. [10.1016/j.physletb.2022.136986]

Availability:
This version is available at: 11583/2971862 since: 2022-09-29T20:07:11Z

Publisher:
ELSEVIER

Published
DOI:10.1016/j.physletb.2022.136986

Terms of use:

This article is made available under terms and conditions as specified in the corresponding bibliographic description in the repository

Publisher copyright

(Article begins on next page)

27 November 2026

Physics Letters B 827 (2022) 136986

Contents lists available at ScienceDirect

Physics Letters B

www.elsevier.com/locate/physletb

Measurement of prompt D_s^+-meson production and azimuthal anisotropy in Pb–Pb collisions at $\sqrt{s_{NN}} = 5.02$ TeV

ALICE Collaboration *

ARTICLE INFO

Article history:
Received 28 October 2021
Received in revised form 27 January 2022
Accepted 18 February 2022
Available online 24 February 2022
Editor: M. Doser

ABSTRACT

The production yield and angular anisotropy of prompt D_s^+ mesons were measured as a function of transverse momentum (p_T) in Pb–Pb collisions at a centre-of-mass energy per nucleon pair $\sqrt{s_{NN}} = 5.02$ TeV collected with the ALICE detector at the LHC. D_s^+ mesons and their charge conjugates were reconstructed at midrapidity ($|y| < 0.5$) from their hadronic decay channel $D_s^+ \to \phi\pi^+$, with $\phi \to K^-K^+$, in the p_T intervals $2 < p_T < 50$ GeV/c and $2 < p_T < 36$ GeV/c for the 0–10% and 30–50% centrality intervals. For $p_T > 10$ GeV/c, the measured D_s^+-meson nuclear modification factor R_{AA} is consistent with the one of non-strange D mesons within uncertainties, while at lower p_T a hint for a D_s^+-meson R_{AA} larger than that of non-strange D mesons is seen. The enhanced production of D_s^+ relative to non-strange D mesons is also studied by comparing the p_T-dependent D_s^+/D^0 production yield ratios in Pb–Pb and in pp collisions. The ratio measured in Pb–Pb collisions is found to be on average higher than that in pp collisions in the interval $2 < p_T < 8$ GeV/c with a significance of 2.3σ and 2.4σ for the 0–10% and 30–50% centrality intervals. The azimuthal anisotropy coefficient v_2 of prompt D_s^+ mesons was measured in Pb–Pb collisions in the 30–50% centrality interval and is found to be compatible with that of non-strange D mesons. The main features of the measured R_{AA}, D_s^+/D^0 ratio, and v_2 as a function of p_T are described by theoretical calculations of charm-quark transport in a hydrodynamically expanding quark–gluon plasma including hadronisation via charm-quark recombination with light quarks from the medium. The p_T-integrated production yield of D_s^+ mesons is compatible with the prediction of the statistical hadronisation model.

© 2022 European Organization for Nuclear Research, ALICE. Published by Elsevier B.V. This is an open access article under the CC BY license (http://creativecommons.org/licenses/by/4.0/). Funded by SCOAP[3].

1. Introduction

Strongly-interacting matter at temperatures exceeding the pseudo-critical value of $T_{pc} \approx 154$–158 MeV and at vanishing baryon density is predicted to behave as a plasma of deconfined quarks and gluons (QGP) [1,2]. A QGP is formed and studied in ultrarelativistic heavy-ion collisions at the CERN Large Hadron Collider (LHC) and existing measurements indicate that it behaves as a strongly-coupled liquid-like system [3]. The lifetime of the QGP produced at the energy densities reached at the LHC is of the order of 10 fm/c [4]. Heavy quarks (charm and beauty) are sensitive probes to investigate the properties of the medium formed in these collisions. Due to their large masses, heavy quarks are produced predominantly in hard partonic scattering processes occurring during the early stages of the collision (i.e. on timescales shorter than the QGP formation time) and therefore experience the entire evolution of the medium. Heavy quarks propagate through the expanding hot and dense medium, interacting and exchanging energy and momentum with its constituents via both inelastic and elastic quantum chromodynamic (QCD) processes. At high momentum, the main effect of these interactions is the energy loss of the heavy quarks in the QGP due to medium-induced gluon radiation and collisional processes. On the other hand, low-momentum heavy quarks, including those shifted to low momentum by the energy loss, probe the diffusion regime dominated by elastic interactions. Since the charm and beauty quark masses are large compared to the medium temperature, the propagation of low-momentum heavy quarks through the fireball can be treated as a "Brownian motion", characterised by many elastic collisions with relatively small momentum transfers [5,6]. As a consequence of the large number of soft collisions with the medium constituents, heavy quarks can acquire significant collective flow when diffusing through the expanding fireball. Due to their large masses, charm quarks have a thermalisation time which is comparable to the fireball lifetime [5,7], and therefore they carry sensitive information on their coupling strength to the expanding medium, preserving memory of the thermalisation process. The process of hadronisation is also predicted to be modified in the presence of the QGP. Once the fireball approaches the pseudo-critical temperature for

* *E-mail address:* alice-publications@cern.ch.

https://doi.org/10.1016/j.physletb.2022.136986
0370-2693/© 2022 European Organization for Nuclear Research, ALICE. Published by Elsevier B.V. This is an open access article under the CC BY license (http://creativecommons.org/licenses/by/4.0/). Funded by SCOAP[3].

the transition to a hadron gas, a significant fraction of low- and intermediate-momentum heavy quarks could hadronise via recombination with other quarks from the medium [8–11], in competition with the fragmentation mechanism, which describes quark-to-hadron transitions in pp, $e^{\pm}p$, and $e^{+}e^{-}$ collisions [12,13].

The effects of the interaction of heavy quarks with the medium are commonly quantified by two main observables: the nuclear modification factor R_{AA} and the elliptic flow v_2. The R_{AA} is defined as the ratio of the transverse-momentum (p_T) differential yields in nucleus–nucleus (AA) collisions and the cross section in proton–proton collisions, scaled by the average nuclear overlap function $\langle T_{AA}\rangle$

$$R_{AA}(p_T) = \frac{1}{\langle T_{AA}\rangle} \times \frac{dN_{AA}/dp_T}{d\sigma_{pp}/dp_T}, \quad (1)$$

where the yield in nucleus–nucleus collisions dN_{AA}/dp_T is measured in a given centrality interval and the $\langle T_{AA}\rangle$ value is proportional to the average number of nucleon–nucleon collisions [14]. The $\langle T_{AA}\rangle$ can be estimated via Glauber-model calculations tuned to match the measured multiplicity distribution of charged particles [15]. The elliptic flow v_2 is the second coefficient of the Fourier expansion of the particle-yield distribution in the azimuthal direction φ relative to the initial-state symmetry plane angle Ψ_2: $v_2 = \langle\cos[2(\varphi - \Psi_2)]\rangle$, where $\langle\rangle$ indicates the average over all particles and all events [16,17].

Measurements of non-strange D-meson production in heavy-ion collisions at RHIC [18] and LHC [19–21] energies show a substantial suppression of the D-meson yields compared to pp collisions at intermediate and high p_T. In central nucleus–nucleus collisions, the R_{AA} exhibits a pronounced drop for $p_T > 4$–5 GeV/c, reaches a minimum around $p_T \approx 8$ GeV/c, and slightly increases at higher p_T. This trend is described by different state-of-the-art model calculations of charm-quark energy loss in the QGP [22–24]. A positive D-meson v_2 is measured at $p_T > 8$–10 GeV/c for semicentral Pb–Pb collisions at the LHC [25,26], and it is understood as originating from the path-length dependence of the charm-quark energy loss in the geometrically anisotropic medium created in collisions with finite impact parameter. At lower p_T, larger values of D-meson v_2 are observed accompanied by a bump-like structure in the R_{AA} reflecting the radial flow of the fireball [19–21]. In particular, the D-meson v_2 for semicentral collisions shows a maximum value at $p_T \approx 3$ GeV/c, a clear mass ordering $v_2(D) < v_2(p) < v_2(\pi)$ at low p_T ($p_T < 3$ GeV/c), and a similar magnitude as the v_2 of charged pions at intermediate p_T ($3 < p_T < 6$ GeV/c) [25,26]. These features are consistent with a scenario in which low-momentum charm quarks acquire a significant collective flow when diffusing through the expanding QGP and hadronise via recombination with light quarks from the medium. The measured R_{AA} and v_2 in this p_T region are described qualitatively, and to some extent also quantitatively, by transport models including charm-quark interactions in a hydrodynamically expanding QGP and hadronisation via both fragmentation and recombination [27–38]. However, a simultaneous description of the nuclear modification factor and the anisotropic flow of D mesons is still a challenge for theoretical models.

Studies of the production of different charm-hadron species, dubbed heavy-flavour hadrochemistry, can provide information on the hadronisation mechanism of charm quarks. In particular, an enhancement of the ground-state charm-strange meson yield relative to that of non-strange D mesons is expected in nucleus–nucleus collisions at low and intermediate momenta as compared to pp interactions, if the dominant process for D-meson formation is the recombination of charm quarks with light quarks from the medium, due to the large abundance of strange quarks in the QGP [39–43]. It was also pointed out in Ref. [43] that the comparison of the v_2 of D_s^+ mesons to that of D mesons without strange-quark content (D^0, D^+, and D^{*+}) could provide sensitivity to the transport properties of the hadronic phase, since D_s^+ mesons are expected to decouple early from the hadron gas and therefore do not pick up significant additional v_2 in the hadronic phase.

The production of D_s^+ mesons was measured at RHIC [44] and the LHC [20,45] in Au–Au and Pb–Pb collisions at different centralities. So far, the results have shown that at low and intermediate p_T the D_s^+/D^0 ratio in central, semicentral, and peripheral collisions is larger than the value measured in pp collisions, though the relatively large uncertainties do not allow firm conclusions. The magnitude and the p_T dependence of the D_s^+/D^0 ratio are captured, at least qualitatively, by models including hadronisation via quark coalescence along with strangeness enhancement in the QGP [33,43,46,47], suggesting a relevant role of recombination processes in the hadronisation of low-momentum charm quarks in the QGP.

In this Letter, we report the measurements of the p_T-differential yield and the nuclear modification factor of prompt D_s^+ mesons in central (0–10%) and semicentral (30–50%) Pb–Pb collisions at $\sqrt{s_{NN}} = 5.02$ TeV, together with the measurement of the prompt D_s^+-meson elliptic flow in semicentral collisions. D_s^+ mesons and their charge conjugates were reconstructed at midrapidity, $|y| < 0.5$, through their hadronic decay channel $D_s^+ \to \phi\pi^+$ with a subsequent decay $\phi \to K^-K^+$. Prompt D_s^+ mesons are defined as those produced directly in the hadronisation of charm quarks or originating from the decays of directly-produced excited open-charm and charmonium states, hence excluding weak decays of beauty hadrons. The data sample used for the analysis reported in this paper was collected with the ALICE detector at the end of 2018 and is larger by a factor of about 8 (4) for central (semicentral) collisions with respect to the sample collected in 2015, used for the previous publications of D_s^+-meson R_{AA} and v_2 [20,48].

2. Experimental apparatus and data sample

The ALICE apparatus comprises a central barrel, which is composed of a set of detectors for charged particle reconstruction and identification at midrapidity, a forward muon spectrometer, and various forward and backward detectors for triggering and event characterisation. A detailed description of the detectors and an overview of their typical performances can be found in Refs. [49,50].

The D_s^+-meson decay candidates and charged conjugates were reconstructed and identified with the central barrel detectors, which cover the full azimuth in the pseudorapidity interval $|\eta| < 0.9$ and are embedded in a large solenoidal magnet providing a homogeneous magnetic field $B = 0.5$ T parallel to the beam direction. Charged-particle trajectories are reconstructed from their hits in the Inner Tracking System (ITS) and the Time Projection Chamber (TPC). The ITS is the innermost detector of the ALICE central barrel, it consists of six cylindrical layers of silicon detectors, allowing a precise determination of the track parameters in the vicinity of the interaction point. The TPC provides track reconstruction with up to 159 three-dimensional space points along the trajectory of a charged particle and provides particle identification via the measurement of the specific ionisation energy loss dE/dx. The Time-Of-Flight (TOF) detector, positioned at a radial distance of about 4 m from the beam axis, extends the particle-identification capabilities of the TPC by measuring the flight time of the charged particles from the interaction point to the TOF. The V0 detector is used for triggering and event selection, as well as for the estimation of the collision centrality and the reference plane for the elliptic flow measurement. It consists of two scintillator arrays, located on both sides of the nominal interaction point and covering the full azimuth in the pseudorapidity intervals $-3.7 < \eta < -1.7$ (V0C) and $2.8 < \eta < 5.1$ (V0A). The neutron Zero Degree Calorime-

ters (ZDC), located along the beam axis on both sides of the central barrel at about 110 m distance from the interaction point, are used for event selection, along with the V0 detector.

The events used in the analysis were recorded with a minimum bias (MB) trigger which required coincident signals in the V0A and V0C detectors. Two additional trigger classes were used to enrich the sample of central and semicentral collisions via an online event selection based on the V0-signal amplitude. Background events due to the interaction of one of the beams with residual gas in the vacuum tube and other machine-induced backgrounds were rejected offline using the V0 and the ZDC timing information [50]. In order to have a uniform acceptance in pseudorapidity, only events with a primary vertex reconstructed within ± 10 cm from the centre of the detector along the beam-line direction were considered in the analysis. Collisions were classified into centrality intervals, defined in terms of percentiles of the hadronic Pb–Pb cross section, based on the V0 signal amplitude, as described in detail in Ref. [51]. Central and semicentral collisions were considered in the analysis of the $\mathrm{D_s^+}$-meson production. The sample of central collisions consists of about 100×10^6 events in the 0–10% centrality interval, corresponding to an integrated luminosity $\mathcal{L}_{\mathrm{int}} \simeq 130\ \mu\mathrm{b}^{-1}$. For semicentral collisions, a sample of about 85×10^6 events in the 30–50% interval was utilised, corresponding to $\mathcal{L}_{\mathrm{int}} \simeq 56\ \mu\mathrm{b}^{-1}$. The average values of the nuclear overlap function, $\langle T_{\mathrm{AA}} \rangle$, for the considered central and semicentral event intervals were estimated via Glauber-model simulations anchored to the measured charged-particle multiplicity distribution, and are $23.26 \pm 0.17\ \mathrm{mb}^{-1}$ and $3.92 \pm 0.06\ \mathrm{mb}^{-1}$ [52], respectively.

The Monte Carlo samples utilised in the analysis were obtained simulating Pb–Pb collisions with the HIJING 1.36 [53] event generator. In each simulated event, additional $\mathrm{c\bar{c}}$- and $\mathrm{b\bar{b}}$-quark pairs were injected using the PYTHIA 8.243 event generator [54,55] (Monash-13 tune [56]) and $\mathrm{D_s^+}$ mesons were forced to decay into the hadronic channel of interest for the analysis. The generated particles were propagated through the detector using the GEANT3 transport package [57]. The conditions of all the ALICE detectors in terms of active channels, gain, noise level, and alignment, and their evolution with time during the data taking period, were taken into account in the simulations.

3. Analysis technique

$\mathrm{D_s^+}$ mesons and their charge conjugates were reconstructed via the decay channel $\mathrm{D_s^+ \to \phi\pi^+ \to K^-K^+\pi^+}$ with branching ratio $\mathrm{BR} = (2.24 \pm 0.08)\%$ [58]. The analysis was based on the reconstruction of decay-vertex topologies displaced from the interaction vertex. The separation induced by the weak decays of prompt $\mathrm{D_s^+}$ mesons is typically a few hundred of μm, $c\tau \simeq 151\ \mu$m [58].

$\mathrm{D_s^+}$-meson candidates were built combining triplets of tracks with the proper charge signs, each with $|\eta| < 0.8$, at least 70 out of 159 crossed TPC pad rows, a fit quality $\chi^2/\mathrm{ndf} < 1.25$ in the TPC (where ndf is the number of degrees of freedom involved in the track fit procedure), and a minimum of two (out of six) hits in the ITS, with at least one in either of the two innermost layers, which provide the best pointing resolution. Moreover, at least 50 clusters available for particle identification (PID) in the TPC were required and only tracks with p_{T} above 0.6 (0.4) GeV/c were considered for central (semicentral) collisions. These track-selection criteria limit the $\mathrm{D_s^+}$-meson acceptance in rapidity, which drops steeply to zero for $|y| > 0.5$ at low p_{T} and for $|y| > 0.8$ at $p_{\mathrm{T}} > 5$ GeV/c. Thus, only $\mathrm{D_s^+}$-meson candidates within a p_{T}-dependent fiducial acceptance region, $|y| < y_{\mathrm{fid}}(p_{\mathrm{T}})$, were selected. The $y_{\mathrm{fid}}(p_{\mathrm{T}})$ value was defined as a second-order polynomial function, increasing from 0.5 to 0.8 in the transverse-momentum range $0 < p_{\mathrm{T}} < 5$ GeV/c, and as a constant term, $y_{\mathrm{fid}} = 0.8$, for $p_{\mathrm{T}} > 5$ GeV/c.

Unlike previous D-meson analyses based on linear selections [20,21,26], a machine-learning (ML) approach based on Boosted Decision Trees (BDT) was adopted for the candidate selection to reduce the large combinatorial background [59]. In particular, the implementation of the BDT algorithm provided by the XGBoost [60] library was employed. Signal samples of prompt $\mathrm{D_s^+}$ mesons for the BDT training were obtained from Monte Carlo simulations as described in Section 2. The background samples were obtained from the sidebands of the candidate invariant-mass distributions in the data. Before the training, loose kinematic and topological selections were applied to the $\mathrm{D_s^+}$-meson candidates together with the PID of decay-product tracks. Pions and kaons were selected by requiring compatibility with the respective particle hypothesis within three times the detector resolution between the measured and the expected signals for either the TPC $\mathrm{d}E/\mathrm{d}x$ or the time of flight. Tracks without TOF hits were identified using only the TPC information. In addition, the absolute difference between the reconstructed $\mathrm{K^+K^-}$ invariant mass and the PDG average mass for the ϕ meson [58] (ΔM_{KK}) was required to be below 15 MeV/c^2. The candidate information provided to the BDTs, as an input for the models to distinguish among prompt $\mathrm{D_s^+}$ mesons and background candidates, was mainly based on the displacement of the tracks from the primary vertex, the distance between the $\mathrm{D_s^+}$-meson decay vertex and the primary vertex, the $\mathrm{D_s^+}$-meson impact parameter, and the cosine of the pointing angle between the $\mathrm{D_s^+}$-meson candidate line of flight (the vector connecting the primary and secondary vertex) and its reconstructed momentum vector. The value of ΔM_{KK} and additional variables related to the PID of decay tracks were also included. Independent BDTs were trained in the different p_{T} intervals of the analysis and for the different centrality intervals. Subsequently, they were applied to the real data sample in which the belonging class, i.e., prompt $\mathrm{D_s^+}$ meson or combinatorial background, of particle candidates is unknown. Selections on the BDT output, which is related to the candidate's probability to be a prompt $\mathrm{D_s^+}$ meson, were optimised to reject a large fraction of the combinatorial background while maintaining high signal-selection efficiency.

3.1. Nuclear modification factor measurement

The raw yields of $\mathrm{D_s^+}$ mesons, including both particles and antiparticles, were extracted from binned maximum-likelihood fits to the invariant-mass distributions. The raw yields could be extracted in transverse-momentum intervals in the ranges $2 < p_{\mathrm{T}} < 50$ GeV/c and $2 < p_{\mathrm{T}} < 36$ GeV/c for the 0–10% and the 30–50% centrality intervals, respectively. The fit function was composed of a Gaussian for the description of the signal and of an exponential term for the background. An additional Gaussian was used to describe the peak due to the decay $\mathrm{D^+ \to K^-K^+\pi^+}$, with a branching ratio of $(9.68 \pm 0.18) \times 10^{-3}$ [58], present at a lower invariant-mass value than the $\mathrm{D_s^+}$-meson signal peak. The statistical significance of the observed signals $S/\sqrt{S+B}$, where S is the raw signal yield obtained by integrating the Gaussian function and B is the background under the peak within 3 standard deviations, varies from 4 to 24 depending on the p_{T} and centrality intervals.

The p_{T}-differential corrected yield of prompt $\mathrm{D_s^+}$ mesons was computed for each p_{T} interval according to

$$\left.\frac{\mathrm{d}N}{\mathrm{d}p_{\mathrm{T}}}\right|_{|y|<0.5} = \frac{1}{2} \times \frac{1}{\Delta p_{\mathrm{T}}} \times \frac{f_{\mathrm{prompt}}(p_{\mathrm{T}}) \times N^{\mathrm{D+\overline{D},raw}}(p_{\mathrm{T}})\big|_{|y|<y_{\mathrm{fid}}(p_{\mathrm{T}})}}{c_{\Delta y}(p_{\mathrm{T}}) \times (\mathrm{Acc} \times \varepsilon)_{\mathrm{prompt}}(p_{\mathrm{T}}) \times \mathrm{BR} \times N_{\mathrm{evt}}}. \quad (2)$$

The raw-yield values $N^{\mathrm{D+\overline{D},raw}}$, which contain the contribution of non-prompt $\mathrm{D_s^+}$ mesons from beauty-hadron decays, were divided

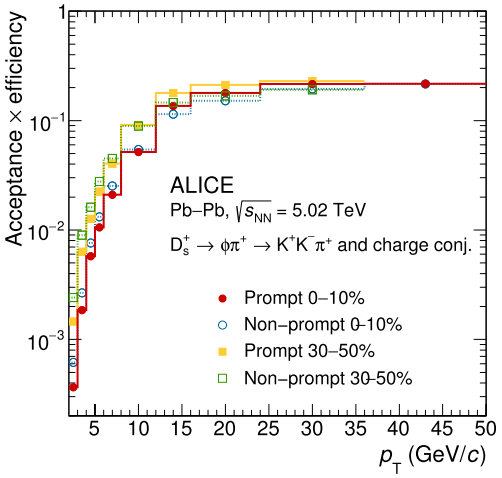

Fig. 1. Acceptance-times-efficiency factor for D_s^+ mesons as a function of p_T. The (Acc $\times$ ε) factors for prompt (red) and non-prompt (blue) D_s^+ mesons in Pb–Pb collisions for the 0–10% centrality interval are shown, together with those for prompt (orange) and non-prompt (green) D_s^+ mesons for the 30–50% centrality interval.

by a factor of two and multiplied by the prompt fraction $f_{\rm prompt}$ to obtain the charge-averaged yields of prompt D_s^+ mesons. Furthermore, they were divided by the acceptance times efficiency of prompt D_s^+ mesons $(\mathrm{Acc}\times\varepsilon)_{\rm prompt}$, the BR of the decay channel, the width of the p_T interval Δp_T, the correction factor for the rapidity coverage $c_{\Delta y}$, and the number of analysed events $N_{\rm evt}$. The correction factor for the rapidity acceptance $c_{\Delta y}$ was computed with FONLL perturbative QCD calculations [61,62]. It was defined as the ratio between the generated D-meson yield in $\Delta y = 2\,y_{\rm fid}$ and that in $|y| < 0.5$. The resulting values were in agreement within 1% with PYTHIA 8 simulations for pp collisions. To account for possible differences in Pb–Pb collisions and as an extreme variation, a flat rapidity distribution was also considered. The discrepancies with respect to FONLL calculations were negligible in comparison to other sources of systematic uncertainty described in Section 4.

The (Acc $\times$ ε) correction was obtained from the simulations described in Section 2 using samples not employed in the BDT training. The D_s^+-meson p_T distributions from simulations were reweighted in order to use realistic momentum distributions in the determination of the (Acc $\times$ ε) factor, which depends on p_T. In particular, the weights were defined to match the shape given by FONLL calculations multiplied by the $R_{\rm AA}$ of D_s^+ mesons predicted by the TAMU [33] model. The (Acc $\times$ ε) factors as a function of p_T for prompt and non-prompt D_s^+ mesons in the 0–10% and 30–50% centrality intervals are shown in Fig. 1. The difference between the (Acc $\times$ ε) factor for prompt and non-prompt D_s^+ mesons arises from the BDT selections applied, given the different decay topology of D_s^+ mesons coming from beauty-hadron decays. In particular, the non-prompt D_s^+ mesons are on average more displaced from the primary vertex due to the large beauty-hadron lifetime, $c\tau \simeq 500$ μm [58], and therefore are more efficiently selected in the low-p_T region. At high p_T, where the candidate decay length is less important to separate signal from background, the BDT selections are able to suppress the non-prompt efficiency with respect to the prompt one. The (Acc $\times$ ε) is higher for semicentral collisions, by up to a factor two at low p_T, since less stringent selections can be applied thanks to the lower combinatorial background.

The $f_{\rm prompt}$ fraction in each p_T interval was obtained following the procedure employed in Refs. [20,21,63]. The calculation was based on the beauty-hadron production cross sections in pp collisions at $\sqrt{s} = 5.02$ TeV from FONLL calculations, the beauty hadron to D + X decay kinematics from the PYTHIA 8 decayer, the (Acc $\times$ ε) correction factor for non-prompt D_s^+ mesons, and the $\langle T_{\rm AA}\rangle$ for the corresponding centrality interval. In addition, the nuclear modification factor of D_s^+ mesons from beauty-hadron decays was accounted for and $R_{\rm AA}^{\rm prompt} = R_{\rm AA}^{\rm non\text{-}prompt}$ was assumed as in Ref. [20]. The values of $f_{\rm prompt}$ range between 0.86 and 0.91 depending on the p_T interval and the centrality interval.

The prompt D_s^+-meson nuclear modification $R_{\rm AA}$ factor was computed following Eq. (1). The measurement of the p_T-differential cross section of prompt D_s^+ mesons with $|y| < 0.5$ in pp collisions at $\sqrt{s} = 5.02$ TeV from Ref. [64], which reaches up to $p_T = 24$ GeV/c, was used as a reference for the $R_{\rm AA}$ computation. At higher D_s^+-meson p_T, $24 < p_T < 50$ GeV/c, FONLL calculations were used as a reference by scaling the predictions to match the measured values at lower p_T. The p_T-extrapolation procedure is the same as in Ref. [63]. As an example, the total systematic uncertainty of the pp reference in the $36 < p_T < 50$ GeV/c interval is $^{+42}_{-33}$%.

3.2. Elliptic flow measurement

The elliptic flow of prompt D_s^+ mesons was measured for semicentral events in transverse-momentum intervals in the range $2 < p_T < 24$ GeV/c. The same ML models trained for the $R_{\rm AA}$ measurement in the 30–50% centrality interval were used and the same selections on the BDT output were applied. The analysis procedure for the v_2 determination followed closely with what was done in Ref. [26] for the measurement of the non-strange D-meson elliptic flow. The D_s^+-meson v_2 coefficients were measured using the Scalar Product (SP) method [65,66] and can be expressed as

$$v_2\{\mathrm{SP}\} = \langle\langle \boldsymbol{u}_2 \cdot \frac{\boldsymbol{Q}_2^{\mathrm{A}*}}{M^{\mathrm{A}}}\rangle\rangle \Big/ \sqrt{\frac{\langle \frac{\boldsymbol{Q}_2^{\mathrm{A}}}{M^{\mathrm{A}}} \cdot \frac{\boldsymbol{Q}_2^{\mathrm{B}*}}{M^{\mathrm{B}}}\rangle \langle \frac{\boldsymbol{Q}_2^{\mathrm{A}}}{M^{\mathrm{A}}} \cdot \frac{\boldsymbol{Q}_2^{\mathrm{C}*}}{M^{\mathrm{C}}}\rangle}{\langle \frac{\boldsymbol{Q}_2^{\mathrm{B}}}{M^{\mathrm{B}}} \cdot \frac{\boldsymbol{Q}_2^{\mathrm{C}*}}{M^{\mathrm{C}}}\rangle}}, \tag{3}$$

where $\boldsymbol{u}_2 = e^{i2\varphi_{\rm D}}$ is the unit flow vector of the D-meson candidate with azimuthal angle $\varphi_{\rm D}$, $\boldsymbol{Q}_2^k$ is the subevent 2$^{\rm nd}$-harmonic flow vector for the subevent k, and M^k represents the subevent multiplicity. The SP denominator was calculated with the formula introduced in Ref. [66], where the three subevents, indicated as A, B, and C, are defined by the particles measured in the V0C, V0A, and TPC detectors, respectively. For the TPC detector, the $\boldsymbol{Q}_2$ vector was computed from the azimuthal angles of charged tracks reconstructed with $|\eta| < 0.8$ and M was the number of measured tracks. For the V0A and V0C detectors, the $\boldsymbol{Q}_2$ vectors were calculated from the azimuthal distribution of the energy deposition in the detector sectors and M was the sum of the amplitudes measured in each channel [26]. The $\boldsymbol{Q}_2$ vectors were corrected for detector effects arising from the non-uniform acceptance [67]. The single bracket $\langle\rangle$ in Eq. (3) refers to an average over all the events, while the double brackets $\langle\langle\rangle\rangle$ denote the average over all particles in the considered p_T interval and all events. The SP denominator was obtained as a function of the collision centrality.

The elliptic flow of D_s^+ mesons cannot be directly measured using Eq. (3) as signal candidates cannot be identified on a particle-by-particle basis. The measured anisotropic flow coefficient $v_2^{\rm tot}$ can be written as a weighted sum of the v_2 of candidates reconstructed from true D_s^+-meson decays ($v_2^{\rm sig}$) and that of the background ($v_2^{\rm bkg}$) [68]

$$v_2^{\rm tot}(M_{\rm D}) = \frac{1}{N^{\rm sig} + N^{\rm bkg} + N^{\rm D^+}}(M_{\rm D}) \times \left[N^{\rm sig}(M_{\rm D})v_2^{\rm sig} + N^{\rm bkg}(M_{\rm D})v_2^{\rm bkg}(M_{\rm D}) + N^{\rm D^+}(M_{\rm D})v_2^{\rm D^+}\right], \tag{4}$$

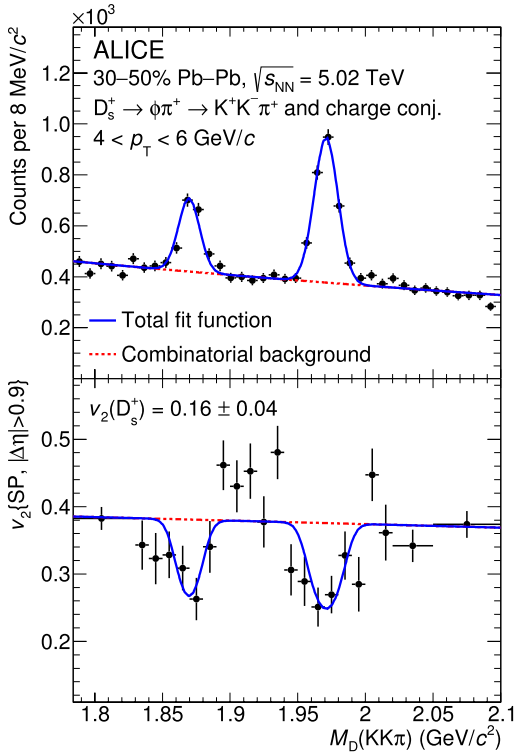

Fig. 2. Simultaneous fit to the invariant-mass spectrum and $v_2(M_{\mathrm{D}})$ of $\mathrm{D_s^+}$-meson candidates in the $4 < p_{\mathrm{T}} < 6$ GeV/c interval for the 30–50% centrality interval. The solid blue and the dotted red curves represent the total and combinatorial-background fit functions, respectively.

where N^{sig} and N^{bkg} are the raw signal and background yields, respectively. An additional $v_2^{\mathrm{D^+}}$ free parameter and the corresponding raw yield $N^{\mathrm{D^+}}$ were included to account for the $\mathrm{D^+ \to K^-K^+\pi^+}$ contribution to the measured v_2^{tot} distribution. A simultaneous fit to the invariant-mass spectrum and the v_2^{tot} distribution as a function of the invariant mass was performed in each p_{T} interval to extract the elliptic flow coefficients. The fit function for the invariant-mass distributions was composed of two Gaussian terms to describe the signal and the peak due to the decay $\mathrm{D^+ \to K^-K^+\pi^+}$, and an exponential distribution for the background, as for the R_{AA} measurement of Section 3.1. The v_2^{sig} was measured from a fit to the v_2^{tot} distribution with the function of Eq. (4), where $v_2^{\mathrm{bkg}}(M_{\mathrm{D}})$ was described by a linear function. Fig. 2 shows the simultaneous fit to the invariant-mass spectrum and $v_2^{\mathrm{tot}}(M_{\mathrm{D}})$ of $\mathrm{D_s^+}$ mesons in the $4 < p_{\mathrm{T}} < 6$ GeV/c interval for the 30–50% centrality interval.

The reconstructed $\mathrm{D_s^+}$-meson signal is a mixture of prompt $\mathrm{D_s^+}$ mesons and non-prompt $\mathrm{D_s^+}$ mesons from beauty-hadron decays. Therefore, the v_2^{sig} can be expressed as a linear combination of prompt (v_2^{prompt}) and non-prompt ($v_2^{\mathrm{non\text{-}prompt}}$) contributions weighted by the fraction of prompt (f_{prompt}) and non-prompt ($1 - f_{\mathrm{prompt}}$) $\mathrm{D_s^+}$ mesons in the extracted signal, respectively. The fraction of promptly produced $\mathrm{D_s^+}$ mesons was estimated as a function of p_{T} with the theory-driven method described in Section 3.1. The v_2 coefficients of prompt $\mathrm{D_s^+}$ mesons were obtained assuming $v_2^{\mathrm{non\text{-}prompt}} = v_2^{\mathrm{prompt}}/2$. This hypothesis is based on the v_2 measurements of the non-prompt J/ψ performed by ATLAS and CMS [69,70], and on the available model calculations [71–73] that indicate $0 < v_2^{\mathrm{non\text{-}prompt}} < v_2^{\mathrm{prompt}}$.

Table 1
Relative systematic uncertainties of the prompt $\mathrm{D_s^+}$-meson corrected yield in Pb–Pb collisions for central and semicentral events in representative p_{T} intervals.

Centrality interval	0–10%		30–50%	
p_{T} (GeV/c)	2–3	12–16	2–3	12–16
Yield extraction	8%	2%	8%	3%
Tracking efficiency	12%	12%	10%	8%
Selection efficiency	9%	4%	5%	3%
Prompt fraction	$^{+8}_{-16}$%	$^{+9}_{-18}$%	$^{+8}_{-16}$%	$^{+8}_{-17}$%
MC p_{T} shape	5%	negl.	3%	negl.
Centrality limits	< 0.1%		2%	
Branching ratio	4%			
Total syst. unc.	$^{+20}_{-24}$%	$^{+16}_{-23}$%	$^{+17}_{-22}$%	$^{+13}_{-20}$%

4. Systematic uncertainties

4.1. Nuclear modification factor measurement

The measurement of the $\mathrm{D_s^+}$-meson corrected yield is affected by the following sources of systematic uncertainties: (i) the raw-yield extraction from the invariant-mass distributions, (ii) the track-reconstruction efficiency, (iii) the PID and selection efficiency, (iv) the generated $\mathrm{D_s^+}$-meson p_{T} shape in the simulation, and (v) the prompt fraction estimation. In addition, the uncertainty due to the branching ratio of 3.6% [58], and that due to the centrality-interval definition were considered. This last contribution arises from the uncertainty of the fraction of the hadronic cross section used in the Glauber fit to determine the centrality, and was estimated to be < 0.1% and 2% for the 0–10% and 30–50% centrality intervals, respectively [63]. A procedure similar to that described in Refs. [20,21] was used to estimate the uncertainties as a function of the p_{T} interval and the centrality interval. The estimated values of the systematic uncertainties are summarised in Table 1 for representative p_{T} intervals, together with the total systematic uncertainty obtained from the sum in quadrature of the different contributions.

The systematic uncertainty of the raw-yield extraction was evaluated by repeating the fit of the invariant- mass distribution varying the lower and upper limits of the fit range, the bin width, and the functional form of the background fit function. The systematic uncertainty was defined as the RMS of the distribution of the signal yields obtained from all these variations and ranges from 2% to 8% depending on the centrality interval and the p_{T} interval.

The systematic uncertainty of the track-reconstruction efficiency was estimated by varying the track- quality selection criteria and by comparing the prolongation probability of the TPC tracks to the ITS hits in data and simulation. The comparison was performed after weighting the relative abundances of primary and secondary particles in the simulation to match those observed in data [74]. The estimated uncertainty ranges from 5% to 14%.

The systematic uncertainty of the selection efficiency originates from imperfections in the description of the detector resolutions and alignments in the simulation. It was estimated by comparing the corrected yields obtained by repeating the analysis with different selections on the BDT output, which resulted in up to 50% higher and lower efficiencies with respect to the central values. The assigned systematic uncertainty ranges from 3% to 9%. Possible systematic effects due to the loose PID selection, applied prior to the machine-learning one, were investigated comparing pion and kaon PID selection efficiencies in data and in simulations. A pure sample of pions was selected from $\mathrm{K^0_S}$ and Λ decays, while samples of kaons in the TPC (TOF) were obtained applying a strict PID selection using the TOF (TPC) information. Since no significant differences were observed, no systematic uncertainty was assigned.

An additional contribution to the systematic uncertainty of the efficiency originates from possible differences between the real

Table 2
Systematic uncertainties of the prompt D_s^+-meson v_2 in Pb–Pb collisions for the 30–50% centrality interval in representative p_T intervals. The uncertainties of the fitting procedure and non-prompt contribution subtraction are quoted as absolute uncertainties, while that of the SP denominator as relative uncertainty.

p_T (GeV/c)	2–4	12–16
M and v_2 fits	0.01	0.02
Non-prompt contribution	$^{+0.031}_{-0.007}$	$^{+0.028}_{-0.006}$
SP denominator	0.5%	

and simulated D_s^+-meson p_T distributions. It was estimated by calculating the efficiency using alternative D_s^+-meson p_T shapes obtained by re-weighting the p_T distribution from MC simulations to match those predicted by theoretical models. The p_T distributions from FONLL calculations including or not hot-medium effects, parametrised using the p_T-differential R_{AA} from the LGR [34], PHSD [75], TAMU [33], and Catania [35] models, were considered. The resulting uncertainty was estimated to be about 5% and 3% for the 0–10% and 30–50% centrality intervals, respectively, in the lowest p_T intervals where the efficiency varies steeply with p_T, and to decrease to zero above 12 GeV/c.

The systematic uncertainty of the prompt fraction was estimated by varying the FONLL parameters (b-quark mass, factorisation, and renormalisation scales, according to the prescription reported in Ref. [76]) in the calculation of the p_T-differential production cross section of non-prompt D_s^+ mesons. In addition, the ratio of the non-prompt and prompt D_s^+-meson R_{AA} was varied in the range $\frac{1}{3} < R_{AA}^{\text{non-prompt}}/R_{AA}^{\text{prompt}} < 3$ as done in Ref. [20]. The resulting uncertainty ranges between $^{+8}_{-16}$% and $^{+12}_{-23}$%.

In the R_{AA} calculation, the BR uncertainty of the D_s^+-meson yield in Pb–Pb collisions and of the pp reference cross section cancels out in the ratio. The contribution due to the prompt fraction uncertainty, estimated by the variation of the parameters of the FONLL calculation, was considered to be fully correlated and the remaining systematic uncertainties were propagated as uncorrelated. The uncertainties of the R_{AA} normalisation are the quadratic sum of the pp normalisation uncertainty, 2.1% [77], the $\langle T_{AA}\rangle$ uncertainty, 0.7% (1.5%) for the 0–10% (30–50%) centrality interval [52], and the one related to the centrality-interval definition described above.

4.2. Elliptic flow measurement

The systematic uncertainties of the measurement of the D_s^+-meson v_2 coefficients were estimated with procedures similar to those detailed in Ref. [26]. They include the following sources: (i) the signal extraction from the invariant-mass and v_2^{tot} distributions, (ii) the non-prompt D_s^+ contribution, and (iii) the centrality dependence of the SP denominator. The selection efficiency was observed to be independent of the D_s^+-meson azimuthal direction, therefore no contribution to the systematic uncertainty was assigned. The non-flow effects are naturally suppressed due to the pseudorapidity gap of at least 0.9 units between the pseudorapidity interval used for the D_s^+-meson reconstruction, and the V0C used for the $\boldsymbol{Q}_2$-vector determination. The estimated values of the systematic uncertainties are summarised in Table 2 for representative p_T intervals.

The uncertainty due to the simultaneous fit was estimated by repeating the fit several times with different configurations, as done for the R_{AA} measurement. The RMS of the v_2 distribution obtained from the different trials, separately for each p_T interval, was assigned as systematic uncertainty. The absolute systematic uncertainty values due to the signal extraction range between 0.01 and 0.03 depending on p_T.

The systematic uncertainty related to the correction for the contribution of non-prompt D_s^+ to the measured v_2 has two main sources. The first one is due to the f_{prompt} calculation and it was treated as described in Section 4.1 for the R_{AA} measurement. The second source is due to the assumption of $v_2^{\text{non-prompt}} = v_2^{\text{prompt}}/2$. This was estimated by considering a flat distribution of $v_2^{\text{non-prompt}}$ between 0 and v_2^{prompt} and by varying the central value of $v_2^{\text{non-prompt}}$ by $\pm v_2^{\text{prompt}}/\sqrt{12}$, corresponding to one standard deviation. The values of the absolute systematic uncertainty from the non-prompt correction range between $^{+0.020}_{-0.005}$ and $^{+0.039}_{-0.009}$ for the different p_T intervals.

The contribution of the SP denominator to the systematic uncertainty is due to the centrality dependence. The uncertainty was evaluated as the difference of the centrality integrated value, computed from the events in the 30–50% interval, with that obtained as weighted average of SP-denominator values in narrow centrality intervals using the D_s^+-meson yields as weights. A systematic uncertainty of 0.5% was assigned.

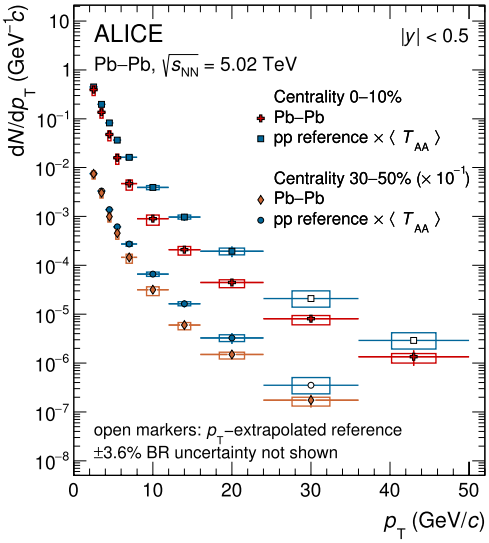

Fig. 3. p_T-differential production yields of prompt D_s^+ mesons in the 0–10% and 30–50% centrality intervals in Pb–Pb collisions at $\sqrt{s_{NN}} = 5.02$ TeV compared to the pp reference [64] scaled by the average nuclear overlap function $\langle T_{AA}\rangle$ of the corresponding centrality interval. The open markers indicate where the pp reference is extrapolated using FONLL calculations. The p_T-differential yields in the 30–50% centrality interval and the corresponding pp reference are scaled by a factor of 10^{-1} for better visibility. Statistical uncertainties (bars) and systematic uncertainties (boxes) are shown.

5. Results

The p_T-differential production yields dN/dp_T of prompt D_s^+ mesons measured in the 0–10% and 30–50% centrality intervals are shown in Fig. 3. For the semicentral class of events, the measurements are scaled by 10^{-1} for better visibility. The results are compared with the pp reference cross section multiplied by the corresponding average nuclear overlap function $\langle T_{AA}\rangle$. The larger data sample and the improved analysis technique enable an extended p_T coverage and finer p_T intervals in the measured dN/dp_T of prompt D_s^+ mesons compared to the previous measurement by the ALICE Collaboration in Pb–Pb collisions at $\sqrt{s_{NN}} = 5.02$ TeV [20]. A strong suppression of the D_s^+ yields compared to the binary-scaled pp reference is observed for both centrality intervals for $p_T > 3$–4 GeV/c, similarly as for the non-strange D mesons [21]. This suppression is understood in terms of modification of the charm-quark momentum spectra due to the interactions within the QGP.

The nuclear modification factor R_{AA} of prompt D_s^+ mesons is compared with the average R_{AA} of prompt D^0, D^+, and D^{*+} mesons in Fig. 4 for the 0–10% and 30–50% centrality intervals, in

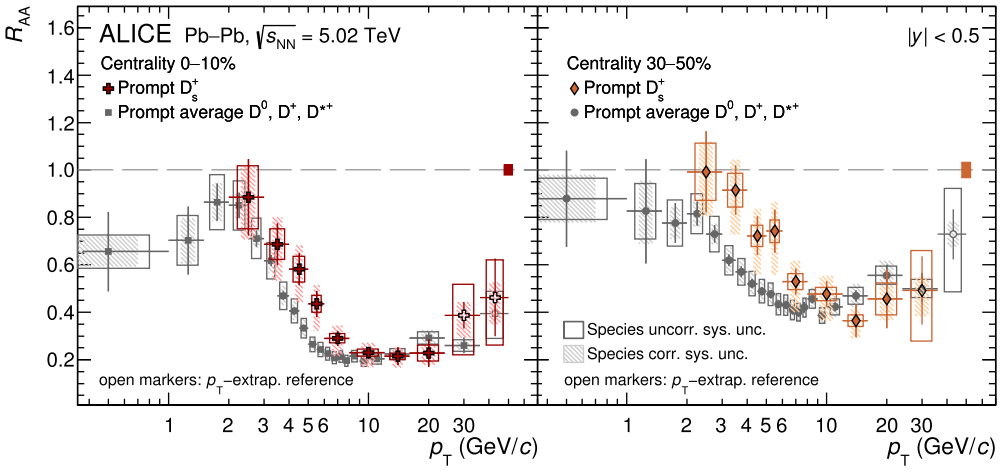

Fig. 4. Nuclear modification factor R_{AA} of prompt D_s^+ mesons in the 0–10% (left panel) and 30–50% (right panel) centrality intervals in Pb–Pb collisions at $\sqrt{s_{NN}} = 5.02$ TeV compared with the one of prompt non-strange D mesons (average of D^0, D^+, and D^{*+}) [21]. The empty (filled) boxes represent the species uncorrelated (correlated) systematic uncertainties. The normalisation uncertainty is represented by a filled box at $R_{AA} = 1$.

the left and right panels, respectively. The systematic uncertainties related to the tracking efficiency and the prompt-fraction estimation are considered as fully correlated between the different D-meson species, and are reported separately from the other sources of systematic uncertainty which are uncorrelated. The R_{AA} of D_s^+ and non-strange D mesons show a minimum value of about 0.2 (0.4) around $p_T \approx 10$ GeV/c in the 0–10% (30–50%) centrality interval. For lower p_T, the R_{AA} increases with decreasing p_T reaching about unity around $p_T \approx 2$–3 GeV/c. In both centrality intervals, the R_{AA} of prompt D_s^+ and non-strange D mesons are compatible within uncertainties for $p_T \gtrsim 10$ GeV/c. In this p_T region, the hadronisation is expected to occur mainly via fragmentation and the dominant effect leading to the observed suppression is the charm-quark energy loss in the QGP. For lower p_T, the measured R_{AA} of prompt D_s^+ mesons is systematically higher than that of non-strange D mesons but compatible within about one standard deviation of the combined statistical and systematic uncertainties.

In the left and right panels of Fig. 5, the R_{AA} of prompt D_s^+ and non-strange D mesons in the 0–10% centrality interval are compared with theoretical calculations implementing charm-quark transport in the QGP [78]. All the models include an enhancement of the strangeness content of the QGP and the hadronisation of charm quarks is implemented either via fragmentation, which is dominant at high p_T, or via coalescence with light quarks in the QGP. In the Catania [35,47] and LGR [34] models the coalescence occurs instantaneously at the phase boundary and is implemented through the Wigner formalism [79]. In the PHSD model [38,75], the hadronisation in heavy-ion collisions is described via a Monte Carlo simulation of the coalescence process in competition to fragmentation. In the TAMU [33] model, the hadronisation via coalescence proceeds via formation of resonant states when approaching the (pseudo)critical temperature within the formalism of a Resonance Recombination Model [11]. For the description of the D-meson p_T spectra in pp collisions, all the models use as starting point FONLL calculations [61,62,76]. Charm quarks are hadronised in pp collisions with fragmentation in the PHSD and LGR models, while in the Catania model the charm-quark hadronisation via coalescence is also implemented in addition to that via fragmentation [80]. In pp collisions, the hadronisation in the TAMU model is instead determined with a statistical hadronisation approach, in which the strangeness production is suppressed in pp with respect to heavy-ion collisions. This is described with a suppression factor for strange particles of $\gamma_s = 0.6$ [81], which is instead unity in heavy-ion collisions. All the models reproduce qualitatively the measured R_{AA} of prompt D_s^+ and non-strange D mesons. The Catania model underestimates both measurements for $2 < p_T < 5$ GeV/c by about 2σ of the combined statistical and systematic uncertainties of the measured points, while it overestimates the non-strange D-meson R_{AA} for $p_T < 1.5$ GeV/c, where no measurement is available for strange mesons. In contrast, the PHSD model describes well the measured nuclear modification factors for $p_T < 5$ GeV/c and underestimates them by about 2σ for higher p_T. The TAMU model describes the measurements within uncertainties, with a tension of about 2σ of the combined statistical and systematic uncertainties of the D_s^+-meson measurement in $2 < p_T < 3$ GeV/c. These three models do not include charm-quark interactions with medium constituents via radiative processes, hence are not expected to describe the R_{AA} of strange and non-strange D mesons for $p_T > 6$–8 GeV/c. The LGR model, which instead includes gluon-radiation processes, provides a good description of the R_{AA} up to high p_T. All the models predict a smaller suppression of the D_s^+-meson R_{AA} compared to non-strange D mesons at low and intermediate p_T.

The possible enhancement of the yield of D mesons with strange-quark content with respect to that of non-strange D mesons was further investigated by computing the ratio between the p_T-differential production yields of prompt D_s^+ mesons and those of prompt D^0 mesons [21]. The systematic uncertainty related to the determination of the tracking efficiency and the contribution due to the subtraction of the component from beauty-hadron decays were propagated as fully correlated in the ratios, while all the other sources of systematic uncertainties were considered as uncorrelated between the measurements of D_s^+ and D^0 mesons. The top row of Fig. 6 shows the D_s^+/D^0 yield ratios in the 0–10% (left panel) and 30–50% (middle panel) centrality intervals compared to the same quantity measured in minimum-bias pp collisions [64] (right panel) and to theoretical calculations. The D_s^+/D^0 yield ratios in Pb–Pb collisions divided by those measured in pp collisions are shown in the bottom row of the same figure. The average values of the D_s^+/D^0 ratios in the $2 < p_T < 8$ GeV/c interval are higher in Pb–Pb collisions than those in pp collisions by about 2.3σ and 2.4σ of the combined statistical and systematic uncertainties, for the 0–10% and 30–50% centrality intervals, respectively. In central collisions, the measured D_s^+/D^0 ratio is compatible with the one measured by the STAR Collaboration in Au–Au collisions at $\sqrt{s_{NN}} = 200$ GeV [44]. The D_s^+/D^0 ratios in pp and in central (central and semicentral) Pb–Pb collisions are described within uncertainties by the Catania (PHSD) model. The TAMU model significantly overestimates the measured D_s^+/D^0 by a similar amount in the two colliding systems, leading to a good de-

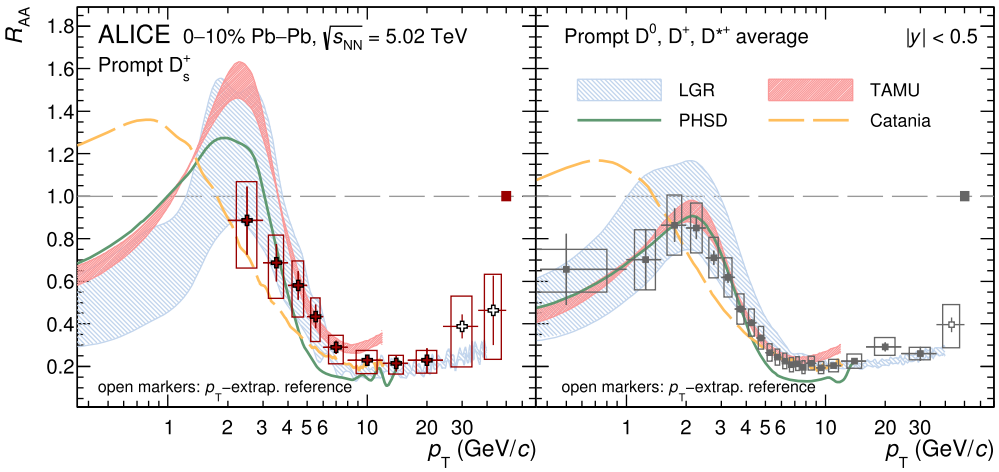

Fig. 5. Nuclear modification factor R_{AA} of prompt D_s^+ mesons (left panel) and non-strange D mesons [21] (right panel) in the 0–10% centrality interval in Pb–Pb collisions at $\sqrt{s_{NN}} = 5.02$ TeV compared with theoretical calculations based on charm-quark transport in a hydrodynamically expanding QGP implementing strangeness enhancement and hadronisation of charm quarks via coalescence in addition to fragmentation in the vacuum [33–35,38,75]. The boxes represent the total systematic uncertainties. The colour bands represent the theoretical uncertainty when available.

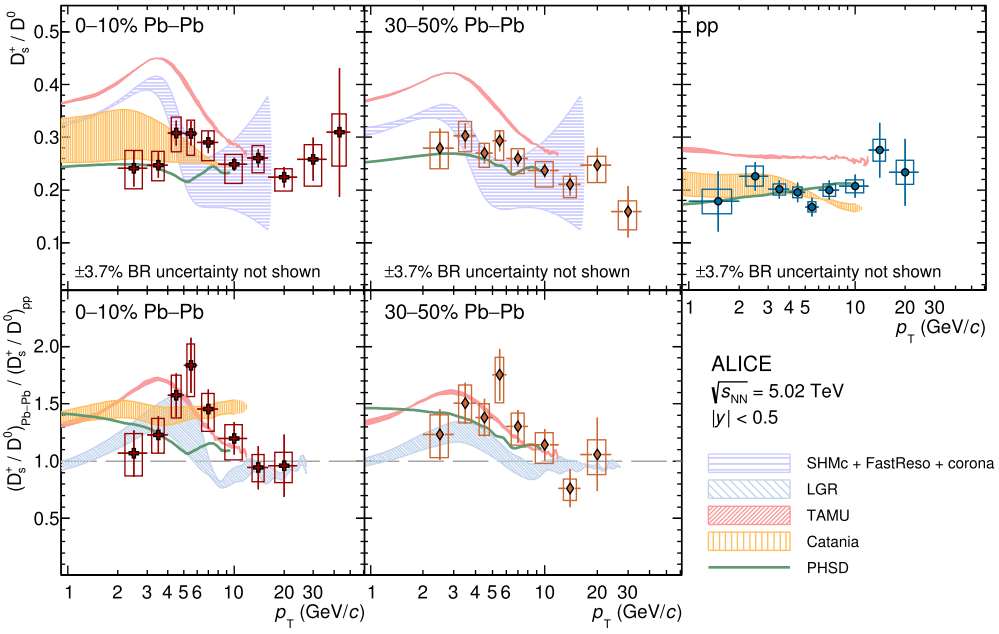

Fig. 6. Top panels: D_s^+/D^0 p_T-differential production ratios in the 0–10% (left panel) and 30–50% (middle panel) centrality intervals in Pb–Pb collisions at $\sqrt{s_{NN}} = 5.02$ TeV and in pp collisions (right panel) at the same centre-of-mass energy compared with theoretical calculations based on charm-quark transport in a hydrodynamically expanding QGP [33,34,38,47,75,80,81] and on statistical hadronisation [82]. Bottom panels: D_s^+/D^0 p_T-differential ratios in Pb–Pb collisions divided by those in pp collisions, in the 0–10% (left panel) and 30–50% (right panel) centrality intervals, compared with theoretical calculations.

scription of the ratio of the D_s^+/D^0 measured in Pb–Pb and pp collisions, as shown in the bottom panels of Fig. 6. While the Catania and PHSD models predict a D_s^+/D^0 ratio almost p_T independent for $p_T < 3$ GeV/c and then mildly decreasing towards the pp value at higher p_T, the TAMU and LGR models predict a peak around $p_T \approx 3$–4 GeV/c. The origin of such a peak would be motivated by the different masses of D_s^+ and D^0 mesons and by the collective radial expansion of the system with a common flow-velocity profile, which imposes an equal velocity boost to all particles in case of complete thermalisation. In addition, also the hadronisation via coalescence is expected to modify the p_T shape of the D_s^+/D^0 ratio due to the different masses of u and s quarks. A similar p_T shape is predicted by the GSI-Heidelberg statistical hadronisation model (SHMc) [82], which is reported in the top panels of Fig. 6 for central and semicentral Pb–Pb collisions, where the p_T spectra of charm hadrons are modelled with a core-corona approach. The low-p_T region is dominated by the core contribution described with a Blast Wave function. The corona contribution is instead parametrised from measurements in pp collisions and is relevant at high p_T. The p_T-spectra modification due to resonance decays is computed using the FastReso package [83]. Within the current uncertainties of the measurement, no firm conclusions can be drawn on the p_T shape of the D_s^+/D^0 ratio in Pb–Pb collisions at low and intermediate p_T. These results however provide important indications about the role of the charm-quark hadronisation via coalescence in the QGP, complementary to those obtained via the simultaneous comparison of the measured D-meson R_{AA} and v_n coefficients [21,26].

The visible production yield of prompt D_s^+ mesons was evaluated by integrating the p_T-differential yield over the narrower p_T intervals of the measurement. The systematic uncertainties were propagated as fully correlated among the measured p_T in-

Table 3
Production yields of prompt D_s^+ mesons in $|y| < 0.5$ in Pb–Pb collisions at $\sqrt{s_{NN}} = 5.02$ TeV compared to the predictions of the GSI-Heidelberg SHMc [82].

Centrality	$dN/dy\|_{\|y\|<0.5}$	GSI-Heidelberg SHMc
0–10%	$1.89 \pm 0.07(\text{stat})^{+0.13}_{-0.16}(\text{syst})^{+0.36}_{-0.55}(\text{extr}) \pm 0.07(\text{BR})$	2.22 ± 0.38
30–50%	$0.34 \pm 0.01(\text{stat})^{+0.02}_{-0.03}(\text{syst})^{+0.11}_{-0.09}(\text{extr}) \pm 0.01(\text{BR})$	0.344 ± 0.056

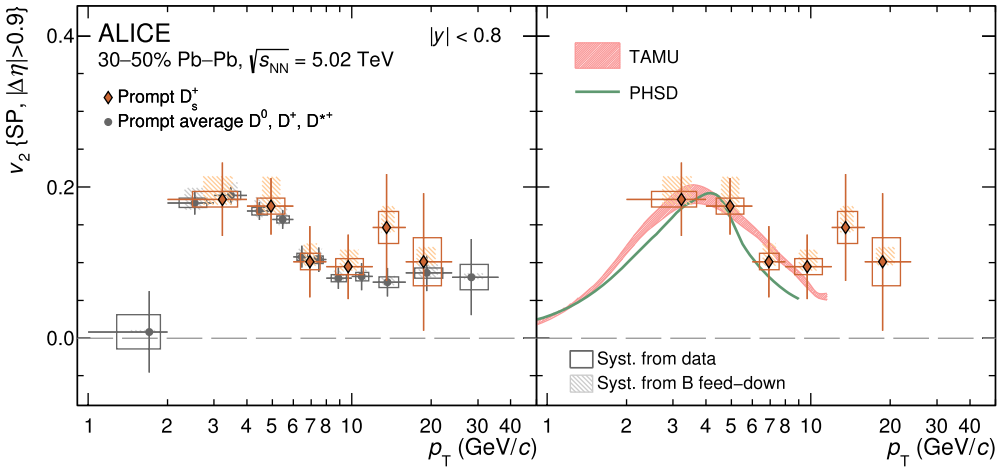

Fig. 7. Elliptic flow coefficient v_2 of prompt D_s^+ mesons in the 30–50% centrality interval in Pb–Pb collisions at $\sqrt{s_{NN}} = 5.02$ TeV compared with that of non-strange D mesons [26] (left panel) and with theoretical calculations based on the charm-quark transport in a hydrodynamically expanding QGP [33,38] (right panel).

tervals, except for the raw-yield extraction uncertainty, which was treated as uncorrelated considering the variations of the signal-to-background ratio and the shape of the combinatorial-background distribution as a function of p_T. In order to obtain the p_T-integrated production yield, the dN/dp_T was extrapolated in $0 < p_T < 2$ GeV/c. For this purpose, the measured p_T-differential D_s^+/D^0 ratio was interpolated using the shape predicted by the PHSD model and leaving the normalisation as a free parameter. The extrapolated D_s^+/D^0 ratio for $p_T < 2$ GeV/c was then multiplied by the dN/dp_T of D^0 mesons measured in the same p_T interval [21] to obtain the extrapolated D_s^+ yield, which amounts to about 70% of the total production yield. An additional uncertainty was assigned to the extrapolation procedure, by repeating the computation using the TAMU and Catania transport models, and the SHMc to extrapolate the D_s^+/D^0 ratio in the unmeasured p_T interval. Finally, the p_T-integrated production yield was obtained as the sum of the extrapolated one for $p_T < 2$ GeV/c and the measured one. The results for the 0–10% and 30–50% centrality intervals are reported in Table 3. As for the D^0, D^+, and D^{*+} mesons [21], the production yield of prompt D_s^+ mesons at midrapidity is compatible within uncertainties with the one predicted by the SHMc. This suggests that low-p_T charm quarks, which determine the total yield, are thermalised in the QGP.

The degree of thermalisation of charm quarks and their hadronisation in the QGP were also studied via the measurement of the azimuthal anisotropy in the prompt D_s^+-meson production. Fig. 7 shows the elliptic flow coefficient v_2 of prompt D_s^+ mesons for the 30–50% centrality interval measured in the transverse-momentum interval $2 < p_T < 24$ GeV/c, compared with that of prompt non-strange D mesons (left panel) and with theoretical calculations (right panel). The rapidity interval of the measurement, $|y| < 0.8$, is wider than that quoted for the R_{AA} since no correction for the rapidity acceptance was applied. The measurement was carried out in finer p_T intervals and has uncertainties reduced by a factor up to four with respect to the previous measurement [48], thanks to the more advanced D_s^+-meson selection technique and the larger data sample. Considering as null hypothesis $v_2 = 0$, the probability to observe the measured positive v_2 in $2 < p_T < 8$ GeV/c corresponds to a significance of 6.4σ, confirming the participation of the charm quark in the collective motion of the system, as already observed for non-strange D mesons [26,48]. However, within the current uncertainties it is not possible to draw a conclusion about a potential difference between the elliptic flow of strange and non-strange D mesons, which would be motivated by the different mass, the charm-quark hadronisation via recombination with strange quarks in the medium instead of light quarks [84], and possible differences in the hadronic phase [43]. The measured D_s^+-meson v_2 is compatible within uncertainties with the predictions of the TAMU and PHSD models, which include charm-quark coalescence with flowing strange quarks in the medium.

6. Summary

In this Letter, a comprehensive and high-precision set of measurements regarding the prompt D_s^+-meson production at midrapidity in Pb–Pb collisions at $\sqrt{s_{NN}} = 5.02$ TeV was reported.

The p_T-differential production yields were measured in a wide transverse-momentum interval between 2–50 (2–36) GeV/c in the 0–10% (30–50%) centrality interval. They were used to compute the p_T-differential R_{AA} and the ratio of D_s^+-meson production relative to D^0 mesons. The measured R_{AA} shows a strong suppression of the D_s^+-meson production yield compared to the binary-scaled pp reference, reaching a minimum of about 0.2 (0.4) around $p_T \approx 10$ GeV/c in the 0–10% (30–50%) centrality interval. For lower p_T, the R_{AA} increases reaching about unity for $p_T \approx 2$–3 GeV/c. The D_s^+/D^0 yield ratios in Pb–Pb collisions are higher than those measured in pp collisions for $p_T \lesssim 8$ GeV/c with a significance of 2.3σ and 2.4σ in the 0–10% and 30–50% centrality intervals, respectively. This finding is consistent with the predictions of theoretical calculations implementing the charm-quark transport in a hydrodynamically expanding QGP, which include an enhanced strange-quark production in the medium and the charm-quark hadronisation via coalescence. The production yield of prompt D_s^+ mesons, extrapolated down to $p_T = 0$, in the 0–10% centrality interval is compatible with the prediction of the SHMc, suggesting that the bulk of charm quarks are thermalised in the QGP.

The elliptic flow coefficient v_2 of prompt D_s^+ mesons was measured as a function of p_T in the 30–50% centrality interval. The D_s^+-meson v_2 in $2 < p_T < 8$ GeV/c is positive with a significance of 6.4σ and is compatible within uncertainties with that of non-strange D mesons. The measured v_2 is also described by several transport-model calculations implementing the charm-quark hadronisation via coalescence.

The data reported in this Letter represent the most precise measurements of prompt D_s^+-meson production in heavy-ion collisions at LHC energies to date, and provide stringent constraints to all models on the production of charm quarks and their hadronisation in the QGP. Future data samples that will be collected with the upgraded ALICE detector in Run 3 will have the potential to further improve and extend to lower p_T the measurement of D_s^+ mesons in heavy-ion collisions [85].

Declaration of competing interest

The authors declare that they have no known competing financial interests or personal relationships that could have appeared to influence the work reported in this paper.

Acknowledgements

The ALICE Collaboration would like to thank all its engineers and technicians for their invaluable contributions to the construction of the experiment and the CERN accelerator teams for the outstanding performance of the LHC complex. The ALICE Collaboration gratefully acknowledges the resources and support provided by all Grid centres and the Worldwide LHC Computing Grid (WLCG) collaboration. The ALICE Collaboration acknowledges the following funding agencies for their support in building and running the ALICE detector: A. I. Alikhanyan National Science Laboratory (Yerevan Physics Institute) Foundation (ANSL), State Committee of Science and World Federation of Scientists (WFS), Armenia; Austrian Academy of Sciences, Austrian Science Fund (FWF): [M 2467-N36] and Nationalstiftung für Forschung, Technologie und Entwicklung, Austria; Ministry of Communications and High Technologies, National Nuclear Research Center, Azerbaijan; Conselho Nacional de Desenvolvimento Científico e Tecnológico (CNPq), Financiadora de Estudos e Projetos (Finep), Fundação de Amparo à Pesquisa do Estado de São Paulo (FAPESP) and Universidade Federal do Rio Grande do Sul (UFRGS), Brazil; Ministry of Education of China (MOEC), Ministry of Science & Technology of China (MSTC) and National Natural Science Foundation of China (NSFC), China; Ministry of Science and Education and Croatian Science Foundation, Croatia; Centro de Aplicaciones Tecnológicas y Desarrollo Nuclear (CEADEN), Cubaenergía, Cuba; The Ministry of Education, Youth and Sports of the Czech Republic, Czech Republic; The Danish Council for Independent Research | Natural Sciences, the Villum Fonden and Danish National Research Foundation (DNRF), Denmark; Helsinki Institute of Physics (HIP), Finland; Commissariat à l'Énergie Atomique (CEA) and Institut National de Physique Nucléaire et de Physique des Particules (IN2P3) and Centre National de la Recherche Scientifique (CNRS), France; Bundesministerium für Bildung und Forschung (BMBF) and GSI Helmholtzzentrum für Schwerionenforschung GmbH, Germany; General Secretariat for Research and Technology, Ministry of Education, Research and Religions, Greece; National Research, Development and Innovation Office, Hungary; Department of Atomic Energy, Government of India (DAE), Department of Science and Technology, Government of India (DST), University Grants Commission, Government of India (UGC) and Council of Scientific and Industrial Research (CSIR), India; Indonesian Institute of Sciences, Indonesia; Istituto Nazionale di Fisica Nucleare (INFN), Italy; Japanese Ministry of Education, Culture, Sports, Science and Technology (MEXT), Japan Society for the Promotion of Science (JSPS) KAKENHI and Japanese Ministry of Education, Culture, Sports, Science and Technology (MEXT) of Applied Science (IIST), Japan; Consejo Nacional de Ciencia (CONACYT) y Tecnología, through Fondo de Cooperación Internacional en Ciencia y Tecnología (FONCICYT) and Dirección General de Asuntos del Personal Académico (DGAPA), Mexico; Nederlandse Organisatie voor Wetenschappelijk Onderzoek (NWO), Netherlands; The Research Council of Norway, Norway; Commission on Science and Technology for Sustainable Development in the South (COMSATS), Pakistan; Pontificia Universidad Católica del Perú, Peru; Ministry of Education and Science, National Science Centre and WUT IDUB, Poland; Korea Institute of Science and Technology Information and National Research Foundation of Korea (NRF), Republic of Korea; Ministry of Education and Scientific Research, Institute of Atomic Physics and Ministry of Research and Innovation and Institute of Atomic Physics, Romania; Joint Institute for Nuclear Research (JINR), Ministry of Education and Science of the Russian Federation, National Research Centre Kurchatov Institute, Russian Science Foundation and Russian Foundation for Basic Research, Russia; Ministry of Education, Science, Research and Sport of the Slovak Republic, Slovakia; National Research Foundation of South Africa, South Africa; Swedish Research Council (VR) and Knut & Alice Wallenberg Foundation (KAW), Sweden; European Organization for Nuclear Research, Switzerland; Suranaree University of Technology (SUT), National Science and Technology Development Agency (NSDTA) and Office of the Higher Education Commission under NRU project of Thailand, Thailand; Turkish Energy, Nuclear and Mineral Research Agency (TENMAK), Turkey; National Academy of Sciences of Ukraine, Ukraine; Science and Technology Facilities Council (STFC), United Kingdom; National Science Foundation of the United States of America (NSF) and United States Department of Energy, Office of Nuclear Physics (DOE NP), United States of America.

References

[1] HotQCD Collaboration, A. Bazavov, et al., Chiral crossover in QCD at zero and non-zero chemical potentials, Phys. Lett. B 795 (2019) 15–21, arXiv:1812.08235 [hep-lat].
[2] S. Borsanyi, Z. Fodor, J.N. Guenther, R. Kara, S.D. Katz, P. Parotto, A. Pasztor, C. Ratti, K.K. Szabo, QCD crossover at finite chemical potential from lattice simulations, Phys. Rev. Lett. 125 (5) (2020) 052001, arXiv:2002.02821 [hep-lat].
[3] W. Busza, K. Rajagopal, W. van der Schee, Heavy ion collisions: the big picture, and the big questions, Annu. Rev. Nucl. Part. Sci. 68 (2018) 339–376, arXiv:1802.04801 [hep-ph].
[4] ALICE Collaboration, K. Aamodt, et al., Two-pion Bose-Einstein correlations in central Pb-Pb collisions at $\sqrt{s_{NN}} = 2.76$ TeV, Phys. Lett. B 696 (2011) 328–337, arXiv:1012.4035 [nucl-ex].
[5] G.D. Moore, D. Teaney, How much do heavy quarks thermalize in a heavy ion collision?, Phys. Rev. C 71 (2005) 064904, arXiv:hep-ph/0412346 [hep-ph].
[6] R. Rapp, H. van Hees, Heavy quark diffusion as a probe of the quark-gluon plasma, arXiv:0803.0901 [hep-ph].
[7] S. Batsouli, S. Kelly, M. Gyulassy, J.L. Nagle, Does the charm flow at RHIC?, Phys. Lett. B 557 (2003) 26–32, arXiv:nucl-th/0212068.
[8] R. Fries, B. Muller, C. Nonaka, S. Bass, Hadronization in heavy ion collisions: recombination and fragmentation of partons, Phys. Rev. Lett. 90 (2003) 202303, arXiv:nucl-th/0301087.
[9] V. Greco, C. Ko, P. Levai, Parton coalescence and anti-proton / pion anomaly at RHIC, Phys. Rev. Lett. 90 (2003) 202302, arXiv:nucl-th/0301093.
[10] V. Greco, C.M. Ko, R. Rapp, Quark coalescence for charmed mesons in ultrarelativistic heavy ion collisions, Phys. Lett. B 595 (2004) 202–208, arXiv:nucl-th/0312100.
[11] L. Ravagli, R. Rapp, Quark coalescence based on a transport equation, Phys. Lett. B 655 (2007) 126–131, arXiv:0705.0021 [hep-ph].
[12] M. Lisovyi, A. Verbytskyi, O. Zenaiev, Combined analysis of charm-quark fragmentation-fraction measurements, Eur. Phys. J. C 76 (7) (2016) 397, arXiv:1509.01061 [hep-ex].
[13] ALICE Collaboration, S. Acharya, et al., Charm-quark fragmentation fractions and production cross section at midrapidity in pp collisions at the LHC, arXiv:2105.06335 [nucl-ex].
[14] X.-N. Wang, Effect of jet quenching on high p_T hadron spectra in high-energy nuclear collisions, Phys. Rev. C 58 (1998) 2321, arXiv:hep-ph/9804357.

[15] M.L. Miller, K. Reygers, S.J. Sanders, P. Steinberg, Glauber modeling in high energy nuclear collisions, Annu. Rev. Nucl. Part. Sci. 57 (2007) 205–243, arXiv:nucl-ex/0701025.

[16] J.-Y. Ollitrault, Anisotropy as a signature of transverse collective flow, Phys. Rev. D 46 (1992) 229–245.

[17] A.M. Poskanzer, S.A. Voloshin, Methods for analyzing anisotropic flow in relativistic nuclear collisions, Phys. Rev. C 58 (1998) 1671–1678, arXiv:nucl-ex/9805001.

[18] STAR Collaboration, J. Adam, et al., Centrality and transverse momentum dependence of D^0-meson production at mid-rapidity in Au+Au collisions at $\sqrt{s_{\rm NN}} = 200$ GeV, Phys. Rev. C 99 (3) (2019) 034908, arXiv:1812.10224 [nucl-ex].

[19] CMS Collaboration, A.M. Sirunyan, et al., Nuclear modification factor of D^0 mesons in PbPb collisions at $\sqrt{s_{\rm NN}} = 5.02$ TeV, Phys. Lett. B 782 (2018) 474–496, arXiv:1708.04962 [nucl-ex].

[20] ALICE Collaboration, S. Acharya, et al., Measurement of D^0, D^+, D^{*+} and D_s^+ production in Pb-Pb collisions at $\sqrt{s_{\rm NN}} = 5.02$ TeV, J. High Energy Phys. 10 (2018) 174, arXiv:1804.09083 [nucl-ex].

[21] ALICE Collaboration, S. Acharya, et al., Prompt D^0, D^+, and D^{*+} production in Pb-Pb collisions at $\sqrt{s_{\rm NN}}$ = 5.02 TeV, arXiv:2110.09420 [nucl-ex].

[22] J. Xu, J. Liao, M. Gyulassy, Consistency of perfect fluidity and jet quenching in semi-quark-gluon monopole plasmas, Chin. Phys. Lett. 32 (9) (2015) 092501, arXiv:1411.3673 [hep-ph].

[23] S. Stojku, B. Ilic, M. Djordjevic, M. Djordjevic, Extracting the temperature dependence in high-$p_\perp$ particle energy loss, Phys. Rev. C 103 (2) (2021) 024908, arXiv:2007.07851 [nucl-th].

[24] Z.-B. Kang, F. Ringer, I. Vitev, Effective field theory approach to open heavy flavor production in heavy-ion collisions, J. High Energy Phys. 03 (2017) 146, arXiv:1610.02043 [hep-ph].

[25] CMS Collaboration, A.M. Sirunyan, et al., Measurement of prompt D^0 meson azimuthal anisotropy in Pb-Pb collisions at $\sqrt{s_{NN}}$ = 5.02 TeV, Phys. Rev. Lett. 120 (20) (2018) 202301, arXiv:1708.03497 [nucl-ex].

[26] ALICE Collaboration, S. Acharya, et al., Transverse-momentum and event-shape dependence of D-meson flow harmonics in Pb–Pb collisions at $\sqrt{s_{NN}}$ = 5.02 TeV, Phys. Lett. B 813 (2021) 136054, arXiv:2005.11131 [nucl-ex].

[27] M. Nahrgang, J. Aichelin, P.B. Gossiaux, K. Werner, Influence of hadronic bound states above T_c on heavy-quark observables in Pb + Pb collisions at at the CERN Large Hadron Collider, Phys. Rev. C 89 (1) (2014) 014905, arXiv:1305.6544 [hep-ph].

[28] R. Katz, C.A.G. Prado, J. Noronha-Hostler, J. Noronha, A.A.P. Suaide, Sensitivity study with a D and B mesons modular simulation code of heavy flavor RAA and azimuthal anisotropies based on beam energy, initial conditions, hadronization, and suppression mechanisms, Phys. Rev. C 102 (2) (2020) 024906, arXiv:1906.10768 [nucl-th].

[29] A. Beraudo, A. De Pace, M. Monteno, M. Nardi, F. Prino, Heavy flavors in heavy-ion collisions: quenching, flow and correlations, Eur. Phys. J. C 75 (3) (2015) 121, arXiv:1410.6082 [hep-ph].

[30] A. Beraudo, A. De Pace, M. Monteno, M. Nardi, F. Prino, Development of heavy-flavour flow-harmonics in high-energy nuclear collisions, J. High Energy Phys. 02 (2018) 043, arXiv:1712.00588 [hep-ph].

[31] S. Cao, T. Luo, G.-Y. Qin, X.-N. Wang, Linearized Boltzmann transport model for jet propagation in the quark-gluon plasma: heavy quark evolution, Phys. Rev. C 94 (1) (2016) 014909, arXiv:1605.06447 [nucl-th].

[32] S. Cao, T. Luo, G.-Y. Qin, X.-N. Wang, Heavy and light flavor jet quenching at RHIC and LHC energies, Phys. Lett. B 777 (2018) 255–259, arXiv:1703.00822 [nucl-th].

[33] M. He, R. Rapp, Hadronization and charm-hadron ratios in heavy-ion collisions, Phys. Rev. Lett. 124 (4) (2020) 042301, arXiv:1905.09216 [nucl-th].

[34] S. Li, J. Liao, Data-driven extraction of heavy quark diffusion in quark-gluon plasma, Eur. Phys. J. C 80 (7) (2020) 671, arXiv:1912.08965 [hep-ph].

[35] F. Scardina, S.K. Das, V. Minissale, S. Plumari, V. Greco, Estimating the charm quark diffusion coefficient and thermalization time from D meson spectra at energies available at the BNL Relativistic Heavy Ion Collider and the CERN Large Hadron Collider, Phys. Rev. C 96 (4) (2017) 044905, arXiv:1707.05452 [nucl-th].

[36] S. Plumari, G. Coci, V. Minissale, S.K. Das, Y. Sun, V. Greco, Heavy - light flavor correlations of anisotropic flows at LHC energies within event-by-event transport approach, Phys. Lett. B 805 (2020) 135460, arXiv:1912.09350 [hep-ph].

[37] W. Ke, Y. Xu, S.A. Bass, Modified Boltzmann approach for modeling the splitting vertices induced by the hot QCD medium in the deep Landau-Pomeranchuk-Migdal region, Phys. Rev. C 100 (6) (2019) 064911, arXiv:1810.08177 [nucl-th].

[38] T. Song, H. Berrehrah, D. Cabrera, J.M. Torres-Rincon, L. Tolos, W. Cassing, E. Bratkovskaya, Tomography of the quark-gluon-plasma by charm quarks, Phys. Rev. C 92 (1) (2015) 014910, arXiv:1503.03039 [nucl-th].

[39] J. Rafelski, B. Muller, Strangeness production in the quark - gluon plasma, Phys. Rev. Lett. 48 (1982) 1066, Phys. Rev. Lett. 56 (1986) 2334, Erratum.

[40] P. Koch, B. Muller, J. Rafelski, Strangeness in relativistic heavy ion collisions, Phys. Rep. 142 (1986) 167–262.

[41] A. Andronic, P. Braun-Munzinger, K. Redlich, J. Stachel, Statistical hadronization of charm in heavy ion collisions at SPS, RHIC and LHC, Phys. Lett. B 571 (2003) 36–44, arXiv:nucl-th/0303036.

[42] I. Kuznetsova, J. Rafelski, Heavy flavor hadrons in statistical hadronization of strangeness-rich QGP, Eur. Phys. J. C 51 (2007) 113–133, arXiv:hep-ph/0607203.

[43] M. He, R.J. Fries, R. Rapp, $\mathbf{D_s}$-meson as quantitative probe of diffusion and hadronization in nuclear collisions, Phys. Rev. Lett. 110 (11) (2013) 112301, arXiv:1204.4442 [nucl-th].

[44] STAR Collaboration, J. Adam, et al., Observation of $D_s^{\pm}/D^0$ enhancement in Au+Au collisions at $\sqrt{s_{\rm NN}}$ = 200 GeV, arXiv:2101.11793 [hep-ex].

[45] ALICE Collaboration, J. Adam, et al., Measurement of D_s^+ production and nuclear modification factor in Pb-Pb collisions at $\sqrt{s_{\rm NN}} = 2.76$ TeV, J. High Energy Phys. 03 (2016) 082, arXiv:1509.07287 [nucl-ex].

[46] J. Zhao, S. Shi, N. Xu, P. Zhuang, Sequential coalescence with charm conservation in high energy nuclear collisions, arXiv:1805.10858 [hep-ph].

[47] S. Plumari, V. Minissale, S.K. Das, G. Coci, V. Greco, Charmed hadrons from coalescence plus fragmentation in relativistic nucleus-nucleus collisions at RHIC and LHC, Eur. Phys. J. C 78 (4) (2018) 348, arXiv:1712.00730 [hep-ph].

[48] ALICE Collaboration, S. Acharya, et al., D-meson azimuthal anisotropy in mid-central Pb-Pb collisions at $\sqrt{\mathbf{s_{\rm NN}}} = \mathbf{5.02}$ TeV, Phys. Rev. Lett. 120 (10) (2018) 102301, arXiv:1707.01005 [nucl-ex].

[49] ALICE Collaboration, K. Aamodt, et al., The ALICE experiment at the CERN LHC, J. Instrum. 3 (2008) S08002.

[50] ALICE Collaboration, B. Abelev, et al., Performance of the ALICE Experiment at the CERN LHC, Int. J. Mod. Phys. A 29 (2014) 1430044, arXiv:1402.4476 [nucl-ex].

[51] ALICE Collaboration, J. Adam, et al., Centrality dependence of the charged-particle multiplicity density at midrapidity in Pb-Pb collisions at $\sqrt{s_{\rm NN}}$ = 5.02 TeV, Phys. Rev. Lett. 116 (22) (2016) 222302, arXiv:1512.06104 [nucl-ex].

[52] ALICE Collaboration, Centrality determination in heavy ion collisions, ALICE-PUBLIC-2018-011, https://cds.cern.ch/record/2636623, Aug 2018.

[53] X.-N. Wang, M. Gyulassy, Hijing: a monte carlo model for multiple jet production in pp, pA, and AA collisions, Phys. Rev. D 44 (Dec 1991) 3501–3516.

[54] T. Sjostrand, S. Mrenna, P.Z. Skands, PYTHIA 6.4 physics and manual, J. High Energy Phys. 05 (2006) 026, arXiv:hep-ph/0603175.

[55] T. Sjöstrand, S. Ask, J.R. Christiansen, R. Corke, N. Desai, P. Ilten, S. Mrenna, S. Prestel, C.O. Rasmussen, P.Z. Skands, An introduction to PYTHIA 8.2, Comput. Phys. Commun. 191 (2015) 159–177, arXiv:1410.3012 [hep-ph].

[56] P. Skands, S. Carrazza, J. Rojo, Tuning PYTHIA 8.1: the Monash 2013 tune, Eur. Phys. J. C 74 (8) (2014) 3024, arXiv:1404.5630 [hep-ph].

[57] R. Brun, F. Bruyant, F. Carminati, S. Giani, M. Maire, A. McPherson, G. Patrick, L. Urban, GEANT: Detector Description and Simulation Tool; Oct 1994, CERN Program Library, CERN, Geneva, 1993, http://cds.cern.ch/record/1082634, Long Writeup W5013.

[58] Particle Data Group Collaboration, P. Zyla, et al., Review of particle physics, PTEP 2020 (8) (2020), 083C01.

[59] L. Barioglio, F. Catalano, M. Concas, P. Fecchio, F. Grosa, F. Mazzaschi, M. Puccio, hipe4ml/hipe4ml, https://doi.org/10.5281/zenodo.5070132, July, 2021.

[60] T. Chen, C. Guestrin, Xgboost: a scalable tree boosting system, in: Proceedings of the 22nd ACM SIGKDD International Conference on Knowledge Discovery and Data Mining, 2016, pp. 785–794, arXiv:1603.02754 [cs.LG].

[61] M. Cacciari, M. Greco, P. Nason, The $p_{\rm T}$ spectrum in heavy-flavor hadroproduction, J. High Energy Phys. 05 (1998) 007, arXiv:hep-ph/9803400 [hep-ph].

[62] M. Cacciari, S. Frixione, P. Nason, The $p_{\rm T}$ spectrum in heavy-flavor photoproduction, J. High Energy Phys. 03 (2001) 006, arXiv:hep-ph/0102134 [hep-ph].

[63] ALICE Collaboration, J. Adam, et al., Transverse momentum dependence of D-meson production in Pb-Pb collisions at $\sqrt{s_{\rm NN}} = 2.76$ TeV, J. High Energy Phys. 03 (2016) 081, arXiv:1509.06888 [nucl-ex].

[64] ALICE Collaboration, S. Acharya, et al., Measurement of beauty and charm production in pp collisions at $\sqrt{s}$ = 5.02 TeV via non-prompt and prompt D mesons, J. High Energy Phys. 05 (2021) 220, arXiv:2102.13601 [nucl-ex].

[65] S.A. Voloshin, A.M. Poskanzer, R. Snellings, Collective phenomena in non-central nuclear collisions, Landolt-Bornstein 23 (2010) 293–333, arXiv:0809.2949 [nucl-ex].

[66] M. Luzum, J.-Y. Ollitrault, Eliminating experimental bias in anisotropic-flow measurements of high-energy nuclear collisions, Phys. Rev. C 87 (4) (2013) 044907, arXiv:1209.2323 [nucl-ex].

[67] I. Selyuzhenkov, S. Voloshin, Effects of non-uniform acceptance in anisotropic flow measurement, Phys. Rev. C 77 (2008) 034904, arXiv:0707.4672 [nucl-th].

[68] N. Borghini, J.Y. Ollitrault, Azimuthally sensitive correlations in nucleus-nucleus collisions, Phys. Rev. C 70 (2004) 064905, arXiv:nucl-th/0407041.

[69] ATLAS Collaboration, M. Aaboud, et al., Prompt and non-prompt J/ψ elliptic flow in Pb+Pb collisions at $\sqrt{s_{\rm NN}} = 5.02$ Tev with the ATLAS detector, Eur. Phys. J. C 78 (9) (2018) 784, arXiv:1807.05198 [nucl-ex].

[70] CMS Collaboration, V. Khachatryan, et al., Suppression and azimuthal anisotropy of prompt and nonprompt J/ψ production in PbPb collisions at $\sqrt{s_{\rm NN}} = 2.76$ TeV, Eur. Phys. J. C 77 (4) (2017) 252, arXiv:1610.00613 [nucl-ex].

[71] J. Uphoff, O. Fochler, Z. Xu, C. Greiner, Open heavy flavor in Pb+Pb collisions at $\sqrt{s} = 2.76$ TeV within a transport model, Phys. Lett. B 717 (2012) 430–435, arXiv:1205.4945 [hep-ph].

[72] J. Aichelin, P.B. Gossiaux, T. Gousset, Radiative and collisional energy loss of heavy quarks in deconfined matter, Acta Phys. Pol. B 43 (2012) 655–662, arXiv:1201.4192 [nucl-th].

[73] V. Greco, H. van Hees, R. Rapp, Heavy-quark kinetics at RHIC and LHC, in: 23rd International Nuclear Physics Conference (INPC 2007), Vol. 9, 2007, arXiv:0709.4452 [hep-ph].
[74] ALICE Collaboration, The ALICE definition of primary particles, ALICE-PUBLIC-2017-005, https://cds.cern.ch/record/2270008, Jun 2017.
[75] T. Song, H. Berrehrah, D. Cabrera, W. Cassing, E. Bratkovskaya, Charm production in Pb + Pb collisions at energies available at the CERN Large Hadron Collider, Phys. Rev. C 93 (3) (2016) 034906, arXiv:1512.00891 [nucl-th].
[76] M. Cacciari, S. Frixione, N. Houdeau, M.L. Mangano, P. Nason, G. Ridolfi, Theoretical predictions for charm and bottom production at the LHC, J. High Energy Phys. 10 (2012) 137, arXiv:1205.6344 [hep-ph].
[77] ALICE Collaboration, ALICE 2017 luminosity determination for pp collisions at $\sqrt{s}$ = 5 TeV, ALICE-PUBLIC-2018-014, http://cds.cern.ch/record/2648933, Nov 2018.
[78] H. Berrehrah, E. Bratkovskaya, T. Steinert, W. Cassing, A dynamical quasiparticle approach for the QGP bulk and transport properties, Int. J. Mod. Phys. E 25 (07) (2016) 1642003, arXiv:1605.02371 [hep-ph].
[79] C.B. Dover, U.W. Heinz, E. Schnedermann, J. Zimanyi, Relativistic coalescence model for high-energy nuclear collisions, Phys. Rev. C 44 (1991) 1636–1654.
[80] V. Minissale, S. Plumari, V. Greco, Charm hadrons in pp collisions at LHC energy within a coalescence plus fragmentation approach, arXiv:2012.12001 [hep-ph].
[81] M. He, R. Rapp, Charm-baryon production in proton-proton collisions, Phys. Lett. B 795 (2019) 117–121, arXiv:1902.08889 [nucl-th].
[82] A. Andronic, P. Braun-Munzinger, M.K. Köhler, A. Mazeliauskas, K. Redlich, J. Stachel, V. Vislavicius, The multiple-charm hierarchy in the statistical hadronization model, J. High Energy Phys. 07 (2021) 035, arXiv:2104.12754 [hep-ph].
[83] A. Mazeliauskas, S. Floerchinger, E. Grossi, D. Teaney, Fast resonance decays in nuclear collisions, Eur. Phys. J. C 79 (3) (2019) 284, arXiv:1809.11049 [nucl-th].
[84] D. Molnar, Charm elliptic flow from quark coalescence dynamics, J. Phys. G 31 (2005) S421–S428, arXiv:nucl-th/0410041.
[85] Z. Citron, et al., Report from Working Group 5: future physics opportunities for high-density QCD at the LHC with heavy-ion and proton beams, CERN Yellow Rep. Monogr. 7 (2019) 1159–1410, arXiv:1812.06772 [hep-ph].

ALICE Collaboration

S. Acharya [143], D. Adamová [98], A. Adler [76], J. Adolfsson [83], G. Aglieri Rinella [35], M. Agnello [31], N. Agrawal [55], Z. Ahammed [143], S. Ahmad [16], S.U. Ahn [78], I. Ahuja [39], Z. Akbar [52], A. Akindinov [95], M. Al-Turany [110], S.N. Alam [16,41], D. Aleksandrov [91], B. Alessandro [61], H.M. Alfanda [7], R. Alfaro Molina [73], B. Ali [16], Y. Ali [14], A. Alici [26], N. Alizadehvandchali [127], A. Alkin [35], J. Alme [21], T. Alt [70], L. Altenkamper [21], I. Altsybeev [115], M.N. Anaam [7], C. Andrei [49], D. Andreou [93], A. Andronic [146], M. Angeletti [35], V. Anguelov [107], F. Antinori [58], P. Antonioli [55], C. Anuj [16], N. Apadula [82], L. Aphecetche [117], H. Appelshäuser [70], S. Arcelli [26], R. Arnaldi [61], I.C. Arsene [20], M. Arslandok [148,107], A. Augustinus [35], R. Averbeck [110], S. Aziz [80], M.D. Azmi [16], A. Badalà [57], Y.W. Baek [42], X. Bai [131,110], R. Bailhache [70], Y. Bailung [51], R. Bala [104], A. Balbino [31], A. Baldisseri [140], B. Balis [2], D. Banerjee [4], R. Barbera [27], L. Barioglio [108], M. Barlou [87], G.G. Barnaföldi [147], L.S. Barnby [97], V. Barret [137], C. Bartels [130], K. Barth [35], E. Bartsch [70], F. Baruffaldi [28], N. Bastid [137], S. Basu [83], G. Batigne [117], B. Batyunya [77], D. Bauri [50], J.L. Bazo Alba [114], I.G. Bearden [92], C. Beattie [148], I. Belikov [139], A.D.C. Bell Hechavarria [146], F. Bellini [26], R. Bellwied [127], S. Belokurova [115], V. Belyaev [96], G. Bencedi [147,71], S. Beole [25], A. Bercuci [49], Y. Berdnikov [101], A. Berdnikova [107], L. Bergmann [107], M.G. Besoiu [69], L. Betev [35], P.P. Bhaduri [143], A. Bhasin [104], I.R. Bhat [104], M.A. Bhat [4], B. Bhattacharjee [43], P. Bhattacharya [23], L. Bianchi [25], N. Bianchi [53], J. Bielčík [38], J. Bielčíková [98], J. Biernat [120], A. Bilandzic [108], G. Biro [147], S. Biswas [4], J.T. Blair [121], D. Blau [91,84], M.B. Blidaru [110], C. Blume [70], G. Boca [29,59], F. Bock [99], A. Bogdanov [96], S. Boi [23], J. Bok [63], L. Boldizsár [147], A. Bolozdynya [96], M. Bombara [39], P.M. Bond [35], G. Bonomi [142,59], H. Borel [140], A. Borissov [84], H. Bossi [148], E. Botta [25], L. Bratrud [70], P. Braun-Munzinger [110], M. Bregant [123], M. Broz [38], G.E. Bruno [109,34], M.D. Buckland [130], D. Budnikov [111], H. Buesching [70], S. Bufalino [31], O. Bugnon [117], P. Buhler [116], Z. Buthelezi [74,134], J.B. Butt [14], A. Bylinkin [129], S.A. Bysiak [120], M. Cai [28,7], H. Caines [148], A. Caliva [110], E. Calvo Villar [114], J.M.M. Camacho [122], R.S. Camacho [46], P. Camerini [24], F.D.M. Canedo [123], F. Carnesecchi [35,26], R. Caron [140], J. Castillo Castellanos [140], E.A.R. Casula [23], F. Catalano [31], C. Ceballos Sanchez [77], P. Chakraborty [50], S. Chandra [143], S. Chapeland [35], M. Chartier [130], S. Chattopadhyay [143], S. Chattopadhyay [112], A. Chauvin [23], T.G. Chavez [46], T. Cheng [7], C. Cheshkov [138], B. Cheynis [138], V. Chibante Barroso [35], D.D. Chinellato [124], S. Cho [63], P. Chochula [35], P. Christakoglou [93], C.H. Christensen [92], P. Christiansen [83], T. Chujo [136], C. Cicalo [56], L. Cifarelli [26], F. Cindolo [55], M.R. Ciupek [110], G. Clai [55,II], J. Cleymans [126,I], F. Colamaria [54], J.S. Colburn [113], D. Colella [109,54,34,147], A. Collu [82], M. Colocci [35], M. Concas [61,III], G. Conesa Balbastre [81], Z. Conesa del Valle [80], G. Contin [24], J.G. Contreras [38], M.L. Coquet [140], T.M. Cormier [99], P. Cortese [32], M.R. Cosentino [125], F. Costa [35], S. Costanza [29,59], P. Crochet [137], R. Cruz-Torres [82], E. Cuautle [71], P. Cui [7], L. Cunqueiro [99], A. Dainese [58], M.C. Danisch [107], A. Danu [69], I. Das [112], P. Das [89], P. Das [4], S. Das [4], S. Dash [50], S. De [89], A. De Caro [30], G. de Cataldo [54], L. De Cilladi [25], J. de Cuveland [40], A. De Falco [23], D. De Gruttola [30], N. De Marco [61], C. De Martin [24], S. De Pasquale [30], S. Deb [51], H.F. Degenhardt [123], K.R. Deja [144], L. Dello Stritto [30], W. Deng [7], P. Dhankher [19], D. Di Bari [34], A. Di Mauro [35], R.A. Diaz [8], T. Dietel [126], Y. Ding [138,7], R. Divià [35], D.U. Dixit [19], Ø. Djuvsland [21], U. Dmitrieva [65], J. Do [63], A. Dobrin [69], B. Dönigus [70], O. Dordic [20], A.K. Dubey [143], A. Dubla [110,93], S. Dudi [103], P. Dupieux [137], N. Dzalaiova [13], T.M. Eder [146], R.J. Ehlers [99], V.N. Eikeland [21], F. Eisenhut [70], D. Elia [54], B. Erazmus [117], F. Ercolessi [26], F. Erhardt [102], A. Erokhin [115], M.R. Ersdal [21], B. Espagnon [80], G. Eulisse [35], D. Evans [113], S. Evdokimov [94], L. Fabbietti [108], M. Faggin [28],

J. Faivre [81], F. Fan [7], A. Fantoni [53], M. Fasel [99], P. Fecchio [31], A. Feliciello [61], G. Feofilov [115], A. Fernández Téllez [46], A. Ferrero [140], A. Ferretti [25], V.J.G. Feuillard [107], J. Figiel [120], S. Filchagin [111], D. Finogeev [65], F.M. Fionda [56,21], G. Fiorenza [35,109], F. Flor [127], A.N. Flores [121], S. Foertsch [74], P. Foka [110], S. Fokin [91], E. Fragiacomo [62], E. Frajna [147], A. Francisco [137], U. Fuchs [35], N. Funicello [30], C. Furget [81], A. Furs [65], J.J. Gaardhøje [92], M. Gagliardi [25], A.M. Gago [114], A. Gal [139], C.D. Galvan [122], P. Ganoti [87], C. Garabatos [110], J.R.A. Garcia [46], E. Garcia-Solis [10], K. Garg [117], C. Gargiulo [35], A. Garibli [90], K. Garner [146], P. Gasik [110], E.F. Gauger [121], A. Gautam [129], M.B. Gay Ducati [72], M. Germain [117], P. Ghosh [143], S.K. Ghosh [4], M. Giacalone [26], P. Gianotti [53], P. Giubellino [110,61], P. Giubilato [28], A.M.C. Glaenzer [140], P. Glässel [107], D.J.Q. Goh [85], V. Gonzalez [145], L.H. González-Trueba [73], S. Gorbunov [40], M. Gorgon [2], L. Görlich [120], S. Gotovac [36], V. Grabski [73], L.K. Graczykowski [144], L. Greiner [82], A. Grelli [64], C. Grigoras [35], V. Grigoriev [96], S. Grigoryan [77,1], F. Grosa [35,61], J.F. Grosse-Oetringhaus [35], R. Grosso [110], G.G. Guardiano [124], R. Guernane [81], M. Guilbaud [117], K. Gulbrandsen [92], T. Gunji [135], W. Guo [7], A. Gupta [104], R. Gupta [104], S.P. Guzman [46], L. Gyulai [147], M.K. Habib [110], C. Hadjidakis [80], G. Halimoglu [70], H. Hamagaki [85], G. Hamar [147], M. Hamid [7], R. Hannigan [121], M.R. Haque [144,89], A. Harlenderova [110], J.W. Harris [148], A. Harton [10], J.A. Hasenbichler [35], H. Hassan [99], D. Hatzifotiadou [55], P. Hauer [44], L.B. Havener [148], S.T. Heckel [108], E. Hellbär [110], H. Helstrup [37], T. Herman [38], E.G. Hernandez [46], G. Herrera Corral [9], F. Herrmann [146], K.F. Hetland [37], H. Hillemanns [35], C. Hills [130], B. Hippolyte [139], B. Hofman [64], B. Hohlweger [93], J. Honermann [146], G.H. Hong [149], D. Horak [38], S. Hornung [110], A. Horzyk [2], R. Hosokawa [15], Y. Hou [7], P. Hristov [35], C. Hughes [133], P. Huhn [70], L.M. Huhta [128], T.J. Humanic [100], H. Hushnud [112], L.A. Husova [146], A. Hutson [127], D. Hutter [40], J.P. Iddon [35,130], R. Ilkaev [111], H. Ilyas [14], M. Inaba [136], G.M. Innocenti [35], M. Ippolitov [91], A. Isakov [38,98], M.S. Islam [112], M. Ivanov [110], V. Ivanov [101], V. Izucheev [94], M. Jablonski [2], B. Jacak [82], N. Jacazio [35], P.M. Jacobs [82], S. Jadlovska [119], J. Jadlovsky [119], S. Jaelani [64], C. Jahnke [124,123], M.J. Jakubowska [144], A. Jalotra [104], M.A. Janik [144], T. Janson [76], M. Jercic [102], O. Jevons [113], A.A.P. Jimenez [71], F. Jonas [99,146], P.G. Jones [113], J.M. Jowett [35,110], J. Jung [70], M. Jung [70], A. Junique [35], A. Jusko [113], J. Kaewjai [118], P. Kalinak [66], A.S. Kalteyer [110], A. Kalweit [35], V. Kaplin [96], A. Karasu Uysal [79], D. Karatovic [102], O. Karavichev [65], T. Karavicheva [65], P. Karczmarczyk [144], E. Karpechev [65], A. Kazantsev [91], U. Kebschull [76], R. Keidel [48], D.L.D. Keijdener [64], M. Keil [35], B. Ketzer [44], Z. Khabanova [93], A.M. Khan [7], S. Khan [16], A. Khanzadeev [101], Y. Kharlov [94,84], A. Khatun [16], A. Khuntia [120], B. Kileng [37], B. Kim [17,63], C. Kim [17], D.J. Kim [128], E.J. Kim [75], J. Kim [149], J.S. Kim [42], J. Kim [107], J. Kim [149], J. Kim [75], M. Kim [107], S. Kim [18], T. Kim [149], S. Kirsch [70], I. Kisel [40], S. Kiselev [95], A. Kisiel [144], J.P. Kitowski [2], J.L. Klay [6], J. Klein [35], S. Klein [82], C. Klein-Bösing [146], M. Kleiner [70], T. Klemenz [108], A. Kluge [35], A.G. Knospe [127], C. Kobdaj [118], M.K. Köhler [107], T. Kollegger [110], A. Kondratyev [77], N. Kondratyeva [96], E. Kondratyuk [94], J. Konig [70], S.A. Konigstorfer [108], P.J. Konopka [35], G. Kornakov [144], S.D. Koryciak [2], A. Kotliarov [98], O. Kovalenko [88], V. Kovalenko [115], M. Kowalski [120], I. Králik [66], A. Kravčáková [39], L. Kreis [110], M. Krivda [113,66], F. Krizek [98], K. Krizkova Gajdosova [38], M. Kroesen [107], M. Krüger [70], E. Kryshen [101], M. Krzewicki [40], V. Kučera [35], C. Kuhn [139], P.G. Kuijer [93], T. Kumaoka [136], D. Kumar [143], L. Kumar [103], N. Kumar [103], S. Kundu [35], P. Kurashvili [88], A. Kurepin [65], A.B. Kurepin [65], A. Kuryakin [111], S. Kushpil [98], J. Kvapil [113], M.J. Kweon [63], J.Y. Kwon [63], Y. Kwon [149], S.L. La Pointe [40], P. La Rocca [27], Y.S. Lai [82], A. Lakrathok [118], M. Lamanna [35], R. Langoy [132], K. Lapidus [35], P. Larionov [35,53], E. Laudi [35], L. Lautner [35,108], R. Lavicka [116,38], T. Lazareva [115], R. Lea [142,24,59], J. Lehrbach [40], R.C. Lemmon [97], I. León Monzón [122], E.D. Lesser [19], M. Lettrich [35,108], P. Lévai [147], X. Li [11], X.L. Li [7], J. Lien [132], R. Lietava [113], B. Lim [17], S.H. Lim [17], V. Lindenstruth [40], A. Lindner [49], C. Lippmann [110], A. Liu [19], D.H. Liu [7], J. Liu [130], I.M. Lofnes [21], V. Loginov [96], C. Loizides [99], P. Loncar [36], J.A. Lopez [107], X. Lopez [137], E. López Torres [8], J.R. Luhder [146], M. Lunardon [28], G. Luparello [62], Y.G. Ma [41], A. Maevskaya [65], M. Mager [35], T. Mahmoud [44], A. Maire [139], M. Malaev [101], N.M. Malik [104], Q.W. Malik [20], L. Malinina [77,IV], D. Mal'Kevich [95], D. Mallick [89], N. Mallick [51], P. Malzacher [110], G. Mandaglio [33,57], V. Manko [91], F. Manso [137], V. Manzari [54], Y. Mao [7], J. Mareš [68], G.V. Margagliotti [24], A. Margotti [55], A. Marín [110], C. Markert [121], M. Marquard [70], N.A. Martin [107], P. Martinengo [35], J.L. Martinez [127], M.I. Martínez [46], G. Martínez García [117], S. Masciocchi [110], M. Masera [25], A. Masoni [56], L. Massacrier [80], A. Mastroserio [141,54], A.M. Mathis [108], O. Matonoha [83], P.F.T. Matuoka [123], A. Matyja [120], C. Mayer [120], A.L. Mazuecos [35], F. Mazzaschi [25], M. Mazzilli [35], M.A. Mazzoni [60,I], J.E. Mdhluli [134], A.F. Mechler [70], F. Meddi [22], Y. Melikyan [65], A. Menchaca-Rocha [73], E. Meninno [116,30], A.S. Menon [127], M. Meres [13], S. Mhlanga [126,74], Y. Miake [136], L. Micheletti [61], L.C. Migliorin [138], D.L. Mihaylov [108], K. Mikhaylov [77,95], A.N. Mishra [147], D. Miśkowiec [110],

A. Modak [4], A.P. Mohanty [64], B. Mohanty [89], M. Mohisin Khan [16,V], M.A. Molander [45], Z. Moravcova [92], C. Mordasini [108], D.A. Moreira De Godoy [146], I. Morozov [65], A. Morsch [35], T. Mrnjavac [35], V. Muccifora [53], E. Mudnic [36], D. Mühlheim [146], S. Muhuri [143], J.D. Mulligan [82], A. Mulliri [23], M.G. Munhoz [123], R.H. Munzer [70], H. Murakami [135], S. Murray [126], L. Musa [35], J. Musinsky [66], J.W. Myrcha [144], B. Naik [134,50], R. Nair [88], B.K. Nandi [50], R. Nania [55], E. Nappi [54], A.F. Nassirpour [83], A. Nath [107], C. Nattrass [133], A. Neagu [20], L. Nellen [71], S.V. Nesbo [37], G. Neskovic [40], D. Nesterov [115], B.S. Nielsen [92], S. Nikolaev [91], S. Nikulin [91], V. Nikulin [101], F. Noferini [55], S. Noh [12], P. Nomokonov [77], J. Norman [130], N. Novitzky [136], P. Nowakowski [144], A. Nyanin [91], J. Nystrand [21], M. Ogino [85], A. Ohlson [83], V.A. Okorokov [96], J. Oleniacz [144], A.C. Oliveira Da Silva [133], M.H. Oliver [148], A. Onnerstad [128], C. Oppedisano [61], A. Ortiz Velasquez [71], T. Osako [47], A. Oskarsson [83], J. Otwinowski [120], M. Oya [47], K. Oyama [85], Y. Pachmayer [107], S. Padhan [50], D. Pagano [142,59], G. Paić [71], A. Palasciano [54], J. Pan [145], S. Panebianco [140], P. Pareek [143], J. Park [63], J.E. Parkkila [128], S.P. Pathak [127], R.N. Patra [104,35], B. Paul [23], H. Pei [7], T. Peitzmann [64], X. Peng [7], L.G. Pereira [72], H. Pereira Da Costa [140], D. Peresunko [91,84], G.M. Perez [8], S. Perrin [140], Y. Pestov [5], V. Petráček [38], M. Petrovici [49], R.P. Pezzi [117,72], S. Piano [62], M. Pikna [13], P. Pillot [117], O. Pinazza [55,35], L. Pinsky [127], C. Pinto [27], S. Pisano [53], M. Płoskoń [82], M. Planinic [102], F. Pliquett [70], M.G. Poghosyan [99], B. Polichtchouk [94], S. Politano [31], N. Poljak [102], A. Pop [49], S. Porteboeuf-Houssais [137], J. Porter [82], V. Pozdniakov [77], S.K. Prasad [4], R. Preghenella [55], F. Prino [61], C.A. Pruneau [145], I. Pshenichnov [65], M. Puccio [35], S. Qiu [93], L. Quaglia [25], R.E. Quishpe [127], S. Ragoni [113], A. Rakotozafindrabe [140], L. Ramello [32], F. Rami [139], S.A.R. Ramirez [46], A.G.T. Ramos [34], T.A. Rancien [81], R. Raniwala [105], S. Raniwala [105], S.S. Räsänen [45], R. Rath [51], I. Ravasenga [93], K.F. Read [99,133], A.R. Redelbach [40], K. Redlich [88,VI], A. Rehman [21], P. Reichelt [70], F. Reidt [35], H.A. Reme-ness [37], R. Renfordt [70], Z. Rescakova [39], K. Reygers [107], A. Riabov [101], V. Riabov [101], T. Richert [83], M. Richter [20], W. Riegler [35], F. Riggi [27], C. Ristea [69], M. Rodríguez Cahuantzi [46], K. Røed [20], R. Rogalev [94], E. Rogochaya [77], T.S. Rogoschinski [70], D. Rohr [35], D. Röhrich [21], P.F. Rojas [46], P.S. Rokita [144], F. Ronchetti [53], A. Rosano [33,57], E.D. Rosas [71], A. Rossi [58], A. Rotondi [29,59], A. Roy [51], P. Roy [112], S. Roy [50], N. Rubini [26], O.V. Rueda [83], R. Rui [24], B. Rumyantsev [77], P.G. Russek [2], R. Russo [93], A. Rustamov [90], E. Ryabinkin [91], Y. Ryabov [101], A. Rybicki [120], H. Rytkonen [128], W. Rzesa [144], O.A.M. Saarimaki [45], R. Sadek [117], S. Sadovsky [94], J. Saetre [21], K. Šafařík [38], S.K. Saha [143], S. Saha [89], B. Sahoo [50], P. Sahoo [50], R. Sahoo [51], S. Sahoo [67], D. Sahu [51], P.K. Sahu [67], J. Saini [143], S. Sakai [136], M.P. Salvan [110], S. Sambyal [104], V. Samsonov [101,96,I], D. Sarkar [145], N. Sarkar [143], P. Sarma [43], V.M. Sarti [108], M.H.P. Sas [148], J. Schambach [99], H.S. Scheid [70], C. Schiaua [49], R. Schicker [107], A. Schmah [107], C. Schmidt [110], H.R. Schmidt [106], M.O. Schmidt [35,107], M. Schmidt [106], N.V. Schmidt [99,70], A.R. Schmier [133], R. Schotter [139], J. Schukraft [35], K. Schwarz [110], K. Schweda [110], G. Scioli [26], E. Scomparin [61], J.E. Seger [15], Y. Sekiguchi [135], D. Sekihata [135], I. Selyuzhenkov [110,96], S. Senyukov [139], J.J. Seo [63], D. Serebryakov [65], L. Šerkšnytė [108], A. Sevcenco [69], T.J. Shaba [74], A. Shabanov [65], A. Shabetai [117], R. Shahoyan [35], W. Shaikh [112], A. Shangaraev [94], A. Sharma [103], H. Sharma [120], M. Sharma [104], N. Sharma [103], S. Sharma [104], U. Sharma [104], O. Sheibani [127], K. Shigaki [47], M. Shimomura [86], S. Shirinkin [95], Q. Shou [41], Y. Sibiriak [91], S. Siddhanta [56], T. Siemiarczuk [88], T.F. Silva [123], D. Silvermyr [83], T. Simantathammakul [118], G. Simonetti [35], B. Singh [108], R. Singh [89], R. Singh [104], R. Singh [51], V.K. Singh [143], V. Singhal [143], T. Sinha [112], B. Sitar [13], M. Sitta [32], T.B. Skaali [20], G. Skorodumovs [107], M. Slupecki [45], N. Smirnov [148], R.J.M. Snellings [64], C. Soncco [114], J. Song [127], A. Songmoolnak [118], F. Soramel [28], S. Sorensen [133], I. Sputowska [120], J. Stachel [107], I. Stan [69], P.J. Steffanic [133], S.F. Stiefelmaier [107], D. Stocco [117], I. Storehaug [20], M.M. Storetvedt [37], P. Stratmann [146], C.P. Stylianidis [93], A.A.P. Suaide [123], T. Sugitate [47], C. Suire [80], M. Sukhanov [65], M. Suljic [35], R. Sultanov [95], V. Sumberia [104], S. Sumowidagdo [52], S. Swain [67], A. Szabo [13], I. Szarka [13], U. Tabassam [14], S.F. Taghavi [108], G. Taillepied [137], J. Takahashi [124], G.J. Tambave [21], S. Tang [137,7], Z. Tang [131], J.D. Tapia Takaki [129,VII], M. Tarhini [117], M.G. Tarzila [49], A. Tauro [35], G. Tejeda Muñoz [46], A. Telesca [35], L. Terlizzi [25], C. Terrevoli [127], G. Tersimonov [3], S. Thakur [143], D. Thomas [121], R. Tieulent [138], A. Tikhonov [65], A.R. Timmins [127], M. Tkacik [119], A. Toia [70], N. Topilskaya [65], M. Toppi [53], F. Torales-Acosta [19], T. Tork [80], S.R. Torres [38], A. Trifiró [33,57], S. Tripathy [55,71], T. Tripathy [50], S. Trogolo [35,28], V. Trubnikov [3], W.H. Trzaska [128], T.P. Trzcinski [144], B.A. Trzeciak [38], A. Tumkin [111], R. Turrisi [58], T.S. Tveter [20], K. Ullaland [21], A. Uras [138], M. Urioni [59,142], G.L. Usai [23], M. Vala [39], N. Valle [29,59], S. Vallero [61], N. van der Kolk [64], L.V.R. van Doremalen [64], M. van Leeuwen [93], P. Vande Vyvre [35], D. Varga [147], Z. Varga [147], M. Varga-Kofarago [147], M. Vasileiou [87], A. Vasiliev [91], O. Vázquez Doce [53,108], V. Vechernin [115], A. Velure [21], E. Vercellin [25], S. Vergara Limón [46], L. Vermunt [64],

R. Vértesi [147], M. Verweij [64], L. Vickovic [36], Z. Vilakazi [134], O. Villalobos Baillie [113], G. Vino [54], A. Vinogradov [91], T. Virgili [30], V. Vislavicius [92], A. Vodopyanov [77], B. Volkel [35,107], M.A. Völkl [107], K. Voloshin [95], S.A. Voloshin [145], G. Volpe [34], B. von Haller [35], I. Vorobyev [108], D. Voscek [119], N. Vozniuk [65], J. Vrláková [39], B. Wagner [21], C. Wang [41], D. Wang [41], M. Weber [116], R.J.G.V. Weelden [93], A. Wegrzynek [35], S.C. Wenzel [35], J.P. Wessels [146], J. Wiechula [70], J. Wikne [20], G. Wilk [88], J. Wilkinson [110], G.A. Willems [146], B. Windelband [107], M. Winn [140], W.E. Witt [133], J.R. Wright [121], W. Wu [41], Y. Wu [131], R. Xu [7], A.K. Yadav [143], S. Yalcin [79], Y. Yamaguchi [47], K. Yamakawa [47], S. Yang [21], S. Yano [47], Z. Yin [7], H. Yokoyama [64], I.-K. Yoo [17], J.H. Yoon [63], S. Yuan [21], A. Yuncu [107], V. Zaccolo [24], C. Zampolli [35], H.J.C. Zanoli [64], N. Zardoshti [35], A. Zarochentsev [115], P. Závada [68], N. Zaviyalov [111], M. Zhalov [101], B. Zhang [7], S. Zhang [41], X. Zhang [7], Y. Zhang [131], V. Zherebchevskii [115], Y. Zhi [11], N. Zhigareva [95], D. Zhou [7], Y. Zhou [92], J. Zhu [7,110], Y. Zhu [7], A. Zichichi [26], G. Zinovjev [3], N. Zurlo [142,59]

[1] *A.I. Alikhanyan National Science Laboratory (Yerevan Physics Institute) Foundation, Yerevan, Armenia*
[2] *AGH University of Science and Technology, Cracow, Poland*
[3] *Bogolyubov Institute for Theoretical Physics, National Academy of Sciences of Ukraine, Kiev, Ukraine*
[4] *Bose Institute, Department of Physics and Centre for Astroparticle Physics and Space Science (CAPSS), Kolkata, India*
[5] *Budker Institute for Nuclear Physics, Novosibirsk, Russia*
[6] *California Polytechnic State University, San Luis Obispo, CA, United States*
[7] *Central China Normal University, Wuhan, China*
[8] *Centro de Aplicaciones Tecnológicas y Desarrollo Nuclear (CEADEN), Havana, Cuba*
[9] *Centro de Investigación y de Estudios Avanzados (CINVESTAV), Mexico City and Mérida, Mexico*
[10] *Chicago State University, Chicago, IL, United States*
[11] *China Institute of Atomic Energy, Beijing, China*
[12] *Chungbuk National University, Cheongju, Republic of Korea*
[13] *Comenius University Bratislava, Faculty of Mathematics, Physics and Informatics, Bratislava, Slovakia*
[14] *COMSATS University Islamabad, Islamabad, Pakistan*
[15] *Creighton University, Omaha, NE, United States*
[16] *Department of Physics, Aligarh Muslim University, Aligarh, India*
[17] *Department of Physics, Pusan National University, Pusan, Republic of Korea*
[18] *Department of Physics, Sejong University, Seoul, Republic of Korea*
[19] *Department of Physics, University of California, Berkeley, CA, United States*
[20] *Department of Physics, University of Oslo, Oslo, Norway*
[21] *Department of Physics and Technology, University of Bergen, Bergen, Norway*
[22] *Dipartimento di Fisica dell'Università 'La Sapienza' and Sezione INFN, Rome, Italy*
[23] *Dipartimento di Fisica dell'Università and Sezione INFN, Cagliari, Italy*
[24] *Dipartimento di Fisica dell'Università and Sezione INFN, Trieste, Italy*
[25] *Dipartimento di Fisica dell'Università and Sezione INFN, Turin, Italy*
[26] *Dipartimento di Fisica e Astronomia dell'Università and Sezione INFN, Bologna, Italy*
[27] *Dipartimento di Fisica e Astronomia dell'Università and Sezione INFN, Catania, Italy*
[28] *Dipartimento di Fisica e Astronomia dell'Università and Sezione INFN, Padova, Italy*
[29] *Dipartimento di Fisica e Nucleare e Teorica, Università di Pavia, Pavia, Italy*
[30] *Dipartimento di Fisica 'E.R. Caianiello' dell'Università and Gruppo Collegato INFN, Salerno, Italy*
[31] *Dipartimento DISAT del Politecnico and Sezione INFN, Turin, Italy*
[32] *Dipartimento di Scienze e Innovazione Tecnologica dell'Università del Piemonte Orientale and INFN Sezione di Torino, Alessandria, Italy*
[33] *Dipartimento di Scienze MIFT, Università di Messina, Messina, Italy*
[34] *Dipartimento Interateneo di Fisica 'M. Merlin' and Sezione INFN, Bari, Italy*
[35] *European Organization for Nuclear Research (CERN), Geneva, Switzerland*
[36] *Faculty of Electrical Engineering, Mechanical Engineering and Naval Architecture, University of Split, Split, Croatia*
[37] *Faculty of Engineering and Science, Western Norway University of Applied Sciences, Bergen, Norway*
[38] *Faculty of Nuclear Sciences and Physical Engineering, Czech Technical University in Prague, Prague, Czech Republic*
[39] *Faculty of Science, P.J. Šafárik University, Košice, Slovakia*
[40] *Frankfurt Institute for Advanced Studies, Johann Wolfgang Goethe-Universität Frankfurt, Frankfurt, Germany*
[41] *Fudan University, Shanghai, China*
[42] *Gangneung-Wonju National University, Gangneung, Republic of Korea*
[43] *Gauhati University, Department of Physics, Guwahati, India*
[44] *Helmholtz-Institut für Strahlen- und Kernphysik, Rheinische Friedrich-Wilhelms-Universität Bonn, Bonn, Germany*
[45] *Helsinki Institute of Physics (HIP), Helsinki, Finland*
[46] *High Energy Physics Group, Universidad Autónoma de Puebla, Puebla, Mexico*
[47] *Hiroshima University, Hiroshima, Japan*
[48] *Hochschule Worms, Zentrum für Technologietransfer und Telekommunikation (ZTT), Worms, Germany*
[49] *Horia Hulubei National Institute of Physics and Nuclear Engineering, Bucharest, Romania*
[50] *Indian Institute of Technology Bombay (IIT), Mumbai, India*
[51] *Indian Institute of Technology Indore, Indore, India*
[52] *Indonesian Institute of Sciences, Jakarta, Indonesia*
[53] *INFN, Laboratori Nazionali di Frascati, Frascati, Italy*
[54] *INFN, Sezione di Bari, Bari, Italy*
[55] *INFN, Sezione di Bologna, Bologna, Italy*
[56] *INFN, Sezione di Cagliari, Cagliari, Italy*
[57] *INFN, Sezione di Catania, Catania, Italy*
[58] *INFN, Sezione di Padova, Padova, Italy*
[59] *INFN, Sezione di Pavia, Pavia, Italy*
[60] *INFN, Sezione di Roma, Rome, Italy*
[61] *INFN, Sezione di Torino, Turin, Italy*
[62] *INFN, Sezione di Trieste, Trieste, Italy*
[63] *Inha University, Incheon, Republic of Korea*

[64] Institute for Gravitational and Subatomic Physics (GRASP), Utrecht University/Nikhef, Utrecht, Netherlands
[65] Institute for Nuclear Research, Academy of Sciences, Moscow, Russia
[66] Institute of Experimental Physics, Slovak Academy of Sciences, Košice, Slovakia
[67] Institute of Physics, Homi Bhabha National Institute, Bhubaneswar, India
[68] Institute of Physics of the Czech Academy of Sciences, Prague, Czech Republic
[69] Institute of Space Science (ISS), Bucharest, Romania
[70] Institut für Kernphysik, Johann Wolfgang Goethe-Universität Frankfurt, Frankfurt, Germany
[71] Instituto de Ciencias Nucleares, Universidad Nacional Autónoma de México, Mexico City, Mexico
[72] Instituto de Física, Universidade Federal do Rio Grande do Sul (UFRGS), Porto Alegre, Brazil
[73] Instituto de Física, Universidad Nacional Autónoma de México, Mexico City, Mexico
[74] iThemba LABS, National Research Foundation, Somerset West, South Africa
[75] Jeonbuk National University, Jeonju, Republic of Korea
[76] Johann-Wolfgang-Goethe Universität Frankfurt Institut für Informatik, Fachbereich Informatik und Mathematik, Frankfurt, Germany
[77] Joint Institute for Nuclear Research (JINR), Dubna, Russia
[78] Korea Institute of Science and Technology Information, Daejeon, Republic of Korea
[79] KTO Karatay University, Konya, Turkey
[80] Laboratoire de Physique des 2 Infinis, Irène Joliot-Curie, Orsay, France
[81] Laboratoire de Physique Subatomique et de Cosmologie, Université Grenoble-Alpes, CNRS-IN2P3, Grenoble, France
[82] Lawrence Berkeley National Laboratory, Berkeley, CA, United States
[83] Lund University Department of Physics, Division of Particle Physics, Lund, Sweden
[84] Moscow Institute for Physics and Technology, Moscow, Russia
[85] Nagasaki Institute of Applied Science, Nagasaki, Japan
[86] Nara Women's University (NWU), Nara, Japan
[87] National and Kapodistrian University of Athens, School of Science, Department of Physics, Athens, Greece
[88] National Centre for Nuclear Research, Warsaw, Poland
[89] National Institute of Science Education and Research, Homi Bhabha National Institute, Jatni, India
[90] National Nuclear Research Center, Baku, Azerbaijan
[91] National Research Centre Kurchatov Institute, Moscow, Russia
[92] Niels Bohr Institute, University of Copenhagen, Copenhagen, Denmark
[93] Nikhef, National institute for subatomic physics, Amsterdam, Netherlands
[94] NRC Kurchatov Institute IHEP, Protvino, Russia
[95] NRC «Kurchatov»Institute – ITEP, Moscow, Russia
[96] NRNU Moscow Engineering Physics Institute, Moscow, Russia
[97] Nuclear Physics Group, STFC Daresbury Laboratory, Daresbury, United Kingdom
[98] Nuclear Physics Institute of the Czech Academy of Sciences, Řež u Prahy, Czech Republic
[99] Oak Ridge National Laboratory, Oak Ridge, TN, United States
[100] Ohio State University, Columbus, OH, United States
[101] Petersburg Nuclear Physics Institute, Gatchina, Russia
[102] Physics department, Faculty of science, University of Zagreb, Zagreb, Croatia
[103] Physics Department, Panjab University, Chandigarh, India
[104] Physics Department, University of Jammu, Jammu, India
[105] Physics Department, University of Rajasthan, Jaipur, India
[106] Physikalisches Institut, Eberhard-Karls-Universität Tübingen, Tübingen, Germany
[107] Physikalisches Institut, Ruprecht-Karls-Universität Heidelberg, Heidelberg, Germany
[108] Physik Department, Technische Universität München, Munich, Germany
[109] Politecnico di Bari and Sezione INFN, Bari, Italy
[110] Research Division and ExtreMe Matter Institute EMMI, GSI Helmholtzzentrum für Schwerionenforschung GmbH, Darmstadt, Germany
[111] Russian Federal Nuclear Center (VNIIEF), Sarov, Russia
[112] Saha Institute of Nuclear Physics, Homi Bhabha National Institute, Kolkata, India
[113] School of Physics and Astronomy, University of Birmingham, Birmingham, United Kingdom
[114] Sección Física, Departamento de Ciencias, Pontificia Universidad Católica del Perú, Lima, Peru
[115] St. Petersburg State University, St. Petersburg, Russia
[116] Stefan Meyer Institut für Subatomare Physik (SMI), Vienna, Austria
[117] SUBATECH, IMT Atlantique, Université de Nantes, CNRS-IN2P3, Nantes, France
[118] Suranaree University of Technology, Nakhon Ratchasima, Thailand
[119] Technical University of Košice, Košice, Slovakia
[120] The Henryk Niewodniczanski Institute of Nuclear Physics, Polish Academy of Sciences, Cracow, Poland
[121] The University of Texas at Austin, Austin, TX, United States
[122] Universidad Autónoma de Sinaloa, Culiacán, Mexico
[123] Universidade de São Paulo (USP), São Paulo, Brazil
[124] Universidade Estadual de Campinas (UNICAMP), Campinas, Brazil
[125] Universidade Federal do ABC, Santo Andre, Brazil
[126] University of Cape Town, Cape Town, South Africa
[127] University of Houston, Houston, TX, United States
[128] University of Jyväskylä, Jyväskylä, Finland
[129] University of Kansas, Lawrence, KS, United States
[130] University of Liverpool, Liverpool, United Kingdom
[131] University of Science and Technology of China, Hefei, China
[132] University of South-Eastern Norway, Tonsberg, Norway
[133] University of Tennessee, Knoxville, TN, United States
[134] University of the Witwatersrand, Johannesburg, South Africa
[135] University of Tokyo, Tokyo, Japan
[136] University of Tsukuba, Tsukuba, Japan
[137] Université Clermont Auvergne, CNRS/IN2P3, LPC, Clermont-Ferrand, France
[138] Université de Lyon, CNRS/IN2P3, Institut de Physique des 2 Infinis de Lyon, Lyon, France
[139] Université de Strasbourg, CNRS, IPHC UMR 7178, F-67000 Strasbourg, France
[140] Université Paris-Saclay Centre d'Etudes de Saclay (CEA), IRFU, Département de Physique Nucléaire (DPhN), Saclay, France
[141] Università degli Studi di Foggia, Foggia, Italy
[142] Università di Brescia, Brescia, Italy
[143] Variable Energy Cyclotron Centre, Homi Bhabha National Institute, Kolkata, India

[144] Warsaw University of Technology, Warsaw, Poland
[145] Wayne State University, Detroit, MI, United States
[146] Westfälische Wilhelms-Universität Münster, Institut für Kernphysik, Münster, Germany
[147] Wigner Research Centre for Physics, Budapest, Hungary
[148] Yale University, New Haven, CT, United States
[149] Yonsei University, Seoul, Republic of Korea

[I] Deceased.
[II] Also at: Italian National Agency for New Technologies, Energy and Sustainable Economic Development (ENEA), Bologna, Italy.
[III] Also at: Dipartimento DET del Politecnico di Torino, Turin, Italy.
[IV] Also at: M.V. Lomonosov Moscow State University, D.V. Skobeltsyn Institute of Nuclear, Physics, Moscow, Russia.
[V] Also at: Department of Applied Physics, Aligarh Muslim University, Aligarh, India.
[VI] Also at: Institute of Theoretical Physics, University of Wroclaw, Poland.
[VII] Also at: University of Kansas, Lawrence, Kansas, United States.